Nonlin. Processes Geophys., 33, 579–604, 2026
https://doi.org/10.5194/npg-33-579-2026
© Author(s) 2026. This work is distributed under
the Creative Commons Attribution 4.0 License.

Nonlinear Processes in Geophysics
Open Access
EGU

Stochastic collection equation: invariant evolution of the cloud droplet–size distribution

Jun-Ichi Yano[1], **Marta Wacławczyk**[2], **and Maarten H. P. Ambaum**[3]

[1]CNRM, UMR 3589 (CNRS), Météo-France, 31057, Toulouse CEDEX, France
[2]Institute of Geophysics, Faculty of Physics, University of Warsaw, Warsaw, Poland
[3]Department of Meteorology, University of Reading, Reading, UK

Correspondence: Jun-Ichi Yano (jun-ichi.yano@cnrs.fr)

Received: 16 June 2026 – Discussion started: 1 July 2026
Revised: 2 November 2026 – Accepted: 9 November 2026 – Published: 26 November 2026

Abstract. The present paper examines the invariant nature of the stochastic collection equation (SCE), which describes the evolution of cloud droplets by coalescence into larger sizes, and eventually to the size of rain droplets. As the main conclusion, the rain formation is *not* a simple consequence of the growth of droplet size. When the given kernel is invariant under a scale transformation, the size distribution of the cloud droplets simply shifts towards larger sizes with time, asymptotically preserving its shape (i.e. *invariance*), and no separate rain peak in the distribution emerges. Findings from the invariance analysis are supported further by numerical experiments. As a corollary, the present study points out that the deviation of a natural collision kernel from *invariance* is a key ingredient for understanding the formation of rain from cloud: a simple demonstration is presented adopting Long's kernel assumption.

1 Introduction

Diffusion growth of cloud droplets beyond the activation point is relatively slow. More efficient growth is achieved by mutual collisions of the droplets, their coalescence into larger sizes, and eventually to the size of rain droplets. This process is described by so–called the stochastic collection equation (SCE). This equation is also referred to as the Smoluchowski (1917) equation in honor of the Polish scientist, who derived it originally. The present paper examines the basic behavior of the stochastic collection equation from the perspective of invariance.

The SCE has already been extensively studied since the pioneering work by Twomey (1964, 1966); Berry (1967); Berry and Reinhardt (1974a, b, c), and its basic behavior has been well established: by running the SCE initialized with a distribution with a single peak at the cloud-droplet scale, a second peak corresponding to larger rain droplets emerges. However, as the present paper is going to point out, such a second peak for rain is not automatically obtained by simply running any SCE: basic physical understanding of the behavior of the SCE is still to be fully developed, although earlier attempts, especially by Berry (1967); Berry and Reinhardt (1974c, d) are well credited.

With this general goal in mind, the present paper examines an aspect of symmetries as mathematical structures of the SCE system. Interest in this aspect of the SCE is emerging today (e.g. Xie, 2024): such an abstract approach helps better interpret the behavior of the SCE simulated numerically. Although the present study only considers some idealized forms of the kernel, the developed methodology of the analysis can, in principle, be applied to more complex and realistic forms of kernel. The abstract analysis also brings basic physical insights of the growth process of clouds, associated with the stochastic collection process.

The present paper more specifically shows that rain formation is *not* a simple consequence of the growth of droplet size: the size distribution of the cloud droplets simply shifts towards larger sizes with time, asymptotically preserving its shape, and no distinguished distribution identified as rain emerges, when the given kernel is *scale invariant*, i.e. the form of the kernel does not change by transforming the scale of the droplet size. The rain droplets identified by a distin-

guished peak in the droplet–size distribution emerge only when a distinguished kernel form is assumed for the rain scale. The present paper demonstrates that, due to the scale invariance of the stochastic collection equation (SCE), the resulting evolution of the size distribution of the droplets does not change by in stretching both time and size, so long as the collision kernel is also scale invariant (i.e. homogeneous: e.g. Fournier and Laurençot, 2006a).

The scale invariance of the SCE can be directly demonstrated by a transformation of variables. This very fact further implies that the behavior of the SCE system does not change by changing the scale of the system, say, by stretching the droplet–mass scale. Some explicit forms of the similarity solutions (cf., Barenblatt, 1996) – the solutions that satisfy the invariances – are further derived by adopting asymptotic expansion methods (cf., Bender and Orszag, 1978). The present paper emphasizes the relevance of the similarity solutions as asymptotic approximations of the system, as also emphasized by Barenblatt (1996), rather than as mathematical artifacts. Here, the same is called the *self–similarity solutions* in mathematics and statistical–physics literature. We adopt the former terminology partially following that of the boundary–layer meteorology (e.g. Sorbjan, 1989). The physical relevance of those similarity solutions is further demonstrated by directly time integrating the SCE numerically, and showing that the droplet–size distribution tends to asymptotically approach these similarity solutions with time, in support of the universality suggested by the invariance analysis.

As a simple implication of the scale invariance of SCE, a conventional distinction between cloud and rain droplets in microphysics does not arise from a simple difference in their sizes. Rather, the difference arises only by introducing either a scale dependence into the collision kernel or another physical process that is not included in the SCE, such as a loss of rain droplets by fall. This final point is numerically demonstrated by adopting Long (1974) idealized kernel in the last section.

The existence of the similarity solutions for the SCE is already well known in the meteorological literature. However, those similarity solutions are often not even mentioned as such, but rather called *self–preserving distributions* (e.g. Friedlander, 1961, see also Sect. 11.7.2 of Pruppacher and Klett, 1997). Moreover, in the literature, the main purpose of adopting the framework of the similarity solutions, or self–preserving distributions is to derive an exact solution of the SCE, as systematically reviewed in e.g. Sects. 11.7 and 15.3 of Pruppacher and Klett (1997). There are also extensive mathematical studies on the *symmetry* structure of the SCE: see e.g. Grigoriev and Meleshko (1995), and Lin et al. (2024); Grigoriev et al. (2010) for an overview of more general subjects. Those studies provide a way of deriving exact similarity solutions of SCE in a general manner. Finally, extensive contributions from mathematics and statistical physics must be acknowledged, as reviewed by e.g. Leyvraz (2003).

To some extent, the present paper translates those already known results in mathematical and statistical–physics literature to the atmospheric–science community, notably for cloud microphysicists. Moreover, the focus of the paper is on the generality of the similarity solutions as approximations rather than as exact solutions: those solutions are suggested to be universal, being derived from the invariance of the system so that physical implications can be further inferred.

An important intention behind the present paper is to demonstrate for cloud microphysicists specifically, and atmospheric scientists and geophysicists more generally, how one can relatively easily examine the structure of a governing equation system of interest at a very basic level without any extensive knowledge of the mathematical theory of symmetries, by taking a particular equation in cloud microphysics. Based on this intention, the present paper avoids the mathematical technicalities of symmetry analysis as much as possible so that it will be accessible with relative ease for the cloud microphysicists, specifically, and geophysicists more generally. For this reason, the following analysis is restricted to the simplest invariance analysis, rather than attempting a complete symmetry analysis. Importantly, the former is sufficient for the present purpose of elucidating the basic invariant nature of the stochastic collection equation (SCE). Yet, we also make our terminologies consistent with that in mathematical symmetry theory as much as possible. The technical terms introduced on this basis are marked by *italics* so that non–mathematical readers would recognize them as special terminologies for the mathematicians.

Being consistent with the above intention, all the mathematical technicalities are moved into the appendices. After listing the variables and notations adopted in the present paper in the Appendix A, the Appendix B discusses the issues of the mass conservation of the system; the Appendix C details the solutions with separation of variables. Most importantly, the Appendix D introduces the basics of the Lie–group transformation approach as well as some important extensions of the analysis of the main text. Under the same spirit, the further numerical analyses are discussed separately in the Appendix E. Importantly, the main text is written in a self–contained manner so that the readers can follow without referring to those Appendices, being consistent with the intention of the paper just outlined. Those Appendices are written for those readers seeking deeper understanding through further analyses.

2 Stochastic Collection Equation

2.1 Formulation

The stochastic collection equation that describes the evolution of the droplet particles by coalescence in terms of its size distribution, $n_*(x_*, t_*)$ is given by:

$$\frac{\partial}{\partial t_*} n_*(x_*, t_*) = \frac{1}{2}\int_0^{x_*} n_*(x_* - y_*, t_*) n_*(y_*, t_*) K_*(x_* - y_*, y_*) \mathrm{d}y_* - n_*(x_*, t_*) \int_0^{+\infty} n_*(y_*, t_*) K_*(x_*, y_*) \mathrm{d}y_*. \quad (1)$$

Here, x_* and t_* are the droplet mass and the time, respectively; $K_*(x_*, y_*)$ is the rate at which two droplets with the masses, x_* and y_*, coalesce into a droplet with the mass, $x_* + y_*$, referred to as collection kernel, or simply *kernel* in the following. Note that the subscript, $*$, is added on all the variables above to designate them to be dimensional, to be contrasted with nondimensional counterparts introduced immediately below without the subscript, $*$.

The first term on the right–hand side of Eq. (1) represents the rate that droplets with the mass, x_*, are generated by coalescence of the two smaller droplet masses, x_{1*} and x_{2*}, with $x_{1*} + x_{2*} = x_*$. Here, this combination can be expressed both as $x_{1*} = x_* - y_*$, $x_{2*} = y_*$ as well as $x_{1*} = y_*$, $x_{2*} = x_* - y_*$. Thus the factor of $1/2$ must be multiplied to account for this redundancy. The second term, in turn, represents the rate that the droplets with mass, x_*, are lost by coalescence with other droplets with the mass, y_*, and growing into larger droplets. These two tendencies define the evolution of the number density, n_*, of a droplet with the mass, x_*. Refer to e.g. Sect. 15.3 of Pruppacher and Klett (1997) for a full discussions. For physically obvious reasons, $K_*(x_*, y_*) \geq 0$ and $K_*(x_*, y_*) = K_*(y_*, x_*)$.

It is physically expected that the total mass, m_* defined by

$$m_* = \int_0^{+\infty} x_* n_*(x_*, t_*) \mathrm{d}x_*, \quad (2)$$

is conserved during droplet coalescence, because the process neither creates nor destroys mass. This is formally shown by multiplying x_* on Eq. (1), and integrating it over the full mass range. However, in this derivation, there is an important condition to be satisfied: the coalescence growth of mass, as defined by

$$\frac{1}{2}\int_0^{X_*} n_*(X_* - y_*, t_*) n_*(y_*, t_*) K_*(X_* - y_*, y_*) \mathrm{d}y_* \quad (3)$$

must vanish as the coalesced mass, X_*, approaches the infinity, i.e. $X_* \to \infty$. However, as will be seen in the following, when the kernel, K_*, increases very fast with increasing masses, x_* and y_*, this condition is not necessarily satisfied, and the system begins to lose mass with time, a phenomenon called *gelation*. See Appendix B for a full exposition. Although mass conservation is assumed in the following analysis, readers should keep this caveat well in mind.

Finally, realize that the term *stochastic collection* is rather a misnomer, because the given formulation does not involve any *stochasticity*. This is in contrast to the so-called super-droplet method (Grabowski et al., 2019), for example, which introduces stochasticity explicitly.

2.2 Nondimensionalization

We nondimensionalize the system by setting:

$$x_* = x_0 x, \quad (4a)$$

$$t = K_0 N_0 t_*, \quad (4b)$$

$$K_*(x_*, y_*) = K_0 K(x, y), \quad (4c)$$

$$x_0 n_*(x_*, t_*) = N_0 n(x, t), \quad (4d)$$

where the variables x, t, K, n designate the nondimensionalized variables using the factors designated by the subscript, 0. We also define the initial total droplet number, N_0, by

$$N_0 = \int_0^{+\infty} n_*(x_*, t_* = 0) \mathrm{d}x_*, \quad (5)$$

This is used to nondimensionalize the droplet–number density, n_*.

We normalize the nondimensional variables by the conditions:

$$\int_0^{+\infty} n(x, t = 0) \mathrm{d}x = 1, \quad (6a)$$

$$\int_0^{+\infty} x n(x, t) \mathrm{d}x = 1. \quad (6b)$$

The first is a direct consequence of the definition (5) above, whereas the second introduces the definition of the droplet–mass scale, x_0, as

$$x_0 = m_*/N_0, \quad (7)$$

where m_* is the total mass defined by Eq. (2).

Substitution of Eqs. (4a)–(4d) into Eq. (1) leads to:

$$\frac{\partial}{\partial t} n(x, t) = \frac{1}{2}\int_0^{x} n(x - y, t) n(y, t) K(x - y, y) \mathrm{d}y - n(x, t) \int_0^{+\infty} n(y, t) K(x, y) \mathrm{d}y. \quad (8)$$

Note that Eq. (8) is identical to the original equation (Eq. 1), apart from the subscripts, $*$, designating dimensional variables in the original. This result implies that the solution of

the SCE is "invariant", i.e. it does not change by the scale of droplet masses. Putting it differently, the form of this distribution does not change by rescaling the size of the droplets. The conclusion here stems from the fact that Eq. (1) does not involve any physical parameters. However, an important condition for this conclusion to follow is that the collection kernel, K, can be treated like one of the dependent variables as in the nondimensionalization here. Thus, the *form invariance* implied here is valid, only if the kernel, K, is by itself, *form invariant* (cf., Kingston and Sophocleous, 1998).

The result also shows that the nondimensionalization merely serves the purpose of normalizing the variables by the conditions (6a, 6b). Note further that the nondimensional total droplet number density, N, is given by

$$N = \int_0^{+\infty} n(x,t)\mathrm{d}x = N_*(t)/N_0 \tag{9}$$

In the following, the nondimensionalized version of SCE (Eq. 8) is considered. Yet, the total mass, $m(=1)$, is occasionally introduced explicitly as a reminder of physical implications of the given statements.

2.3 Separation of Variables

One of the most basic procedures to solve a multi–variable integro–differential equation is to seek a solution with separation of variables with the form

$$n(x,t) = \tilde{N}(t)\tilde{n}(x). \tag{10}$$

However, as detailed in the Appendix C, the separation of variables given by Eq. (10) does not lead to any consistent solution. Lack of a consistent solution can be explained also from a physical basis: we expect that the peak of the distribution, n, would move to a larger size with time by following the coalescence growth of the droplets. Thus, a "stationary" solution for n, as defined by separation of variables (10), is not feasible.

3 Invariance Analysis: Invariant Transforms

To elucidate the invariance of the SCE by changing the scales as already implied by the nondimensionalization in Sect. 2 further, we now identify the basic invariance properties of SCE. The invariance analysis presented herein is a special case of more general symmetry analysis as presented by e.g. Bluman and Kumei (1989) and Grigoriev et al. (2010). A systematic symmetry analysis based on the Lie group (cf., Appendix D) is already performed by e.g. Grigoriev and Meleshko (1995); Lin et al. (2024). Here, we focus on the *invariant transformations* that do not change the form of the SCE.

Thus, we seek the transformation of the variables of the form

$$x^* = x/x_r, \tag{11a}$$
$$t^* = t/t_r, \tag{11b}$$
$$K^* = K/K_r, \tag{11c}$$
$$n^* = n/n_r, \tag{11d}$$

that keep the governing equation (SCE) invariant. Here, the transformed variables are designated by * signs, and constants for transformations by the subscript r. Importantly, the transformation of the kernel given by Eq. (11c) is a provisional one, or alternatively put it, hypothetical one. In reality, the kernel is transformed by following the transformation of mass, given by Eq. (11a), thus the transformation constant, K_r, cannot be chosen freely. However, by transforming the kernel in this manner with a constant, K_r, we can identify contribution of the kernel, that is required to maintain the invariance, in the equation more explicitly. The constraint on the constant, K_r, due to its dependence on the mass, x and y, is given later by Eq. (16), which is incorporated into the other constraints already obtained. This type of "incomplete" transformation rules are more precisely called the *equivalence transformations*: see chap. 6 of Bluman and Kumei (1989) for importance of this concept.

Similarity of the transformation rules (11a–11d) to the nondimensionalization procedure, defined by Eqs. (4a)–(4d), is worthwhile to note: a close link of the two operations can be shown in a more formal manner (cf., chap. 1 of Bluman and Kumei, 1989). Also recall that the adopted nondimensionalization keeps the governing equation (SCE) *form invariant*. The goal here is to identify a more general transformation rule to maintain an invariance.

By substituting the transformations (11a)–(11d) into Eq. (8), we obtain:

$$\frac{n_r}{t_r}\frac{\partial}{\partial t^*}n^*(x^*,t^*) = n_r^2 K_r x_r \left[\frac{1}{2}\int_0^{x^*} n^*(x^*-y^*,t^*)n^*(y^*,t^*)K^*(x^*-y^*,y^*)\mathrm{d}y^* - n^*(x^*,t^*)\int_0^{+\infty} n^*(y^*,t^*)K^*(x^*,y^*)\mathrm{d}y^*\right]. \tag{12}$$

Comparing the left- and right-hand sides shows that for the transformation constants to drop out of the final result, the scaling factors on both sides must be equal, i.e.

$$\frac{n_r}{t_r} = n_r^2 K_r x_r.$$

Thus, we identify the condition for the invariant *equivalence* transformation as:

$$n_r K_r x_r t_r = 1. \tag{13a}$$

It may particularly be worthwhile to re–write the above constraint into the form,

$$K_r = \frac{1}{n_r x_r t_r}. \tag{13b}$$

This expression explicitly shows how the kernel scale must be adjusted by following the transformations of the scales of other variables.

A special case to consider is when only the transformations in time (Eq. 11b) and of the number density (Eq. 11d) are retained by setting $K_r = 1$ and $x_r = 1$. As a result, the condition (13a) reduces to:

$$n_r t_r = 1. \tag{14a}$$

This constraint means that when the time is stretched by a factor, c, the number density must be reduced as a whole by the factor, $1/c$, i.e.

$$t^* = ct, n^* = n/c. \tag{14b}$$

This invariant transformation is originally explicitly pointed out by Srivastava (1988), although earlier papers implicitly invoke this rule.

Another constraint on invariant transformation is obtained by further introducing the transformation of the total mass by

$$m^* = m/m_r. \tag{15a}$$

From the conservation of mass (Eq. 3), we obtain the constraint:

$$x_r^2 n_r = m_r. \tag{15b}$$

This result summarizes Eqs. (2)–(4) of Xie (2024).

Especially, when we seek a transformation of the time from $t = t_1$ to $t = t_2$ as an actual evolution of the system, m_r must be kept constant, because the total mass does not change with time. In this case, without loss of generality, we set $m_r = 1$, and

$$x_r^2 n_r = 1. \tag{15c}$$

In the following, we focus on this case in seeking invariant solutions that can describe an actual evolution of the distribution. Equation (15c) can be re-interpreted as a definition of n_r in terms of x_r:

$$n_r = 1/x_r^2. \tag{15d}$$

By substituting Eq. (15d) into Eq. (13a), we find

$$K_r t_r / x_r = 1. \tag{15e}$$

Now, recall that the kernel transformation is more precisely defined by the transformation (11a) of the mass. Here, we assume a homogeneous form (cf., Fournier and Laurençot, 2006a),

$$K_r = x_r^\gamma, \tag{16}$$

with the transformation constant, K_r, of the kernel, where γ is a constant to be specified based on a given form of the kernel. Note that adding Eq. (16) to already–introduced transformation rules, Eqs. (11a)–(11d), constitutes a *symmetry transformation*.

By further substituting Eq. (16) into Eq. (15e), we obtain:

$$t_r = x_r^{1-\gamma}, \tag{17a}$$

or alternatively,

$$x_r = t_r^{1/(1-\gamma)}, \tag{17b}$$

when $\gamma \neq 1$. By further substituting Eq. (17b) into Eq. (15d), we also obtain:

$$n_r = 1/t_r^{2/(1-\gamma)}, \tag{17c}$$

when $\gamma \neq 1$. The transformations, (17b) and (17c), or (17a) and (15d), constitutes two possible pairs for defining the invariant transformations. In the following, we focus on the first pair, Eqs. (17b) and (17c), for ease of interpretations, except the case with $\gamma = 1$ when the transformation (17c) is ill-defined. In this case, we adopt the latter pair, Eqs. (17a) and (15d).

The constraint (17a) suggests an invariant relation:

$$t x^{\gamma-1} = t^* x^{*\gamma-1}.$$

This invariant relation further suggests that these two independent variables, t and x, can be combined into a single independent variable,

$$\xi = t x^{\gamma-1}, \tag{18a}$$

or alternatively, from Eq. (17b),

$$\xi = x t^{1/(\gamma-1)}, \tag{18b}$$

when $\gamma \neq 1$. In the following, ξ is defined by Eq. (18b), and interpreted as a transformed droplet mass, except for the case with $\gamma = 1$. In the latter case, we follow Eq. (18a).

In the same manner, the constraint (17c) suggests the invariant relation,

$$n t^{2/(1-\gamma)} = n^* t^{*2/(1-\gamma)}, \tag{19a}$$

and suggest to introduce a new dependent variable by

$$\nu = n t^{2/(1-\gamma)}, \tag{19b}$$

when $\gamma \neq 1$. By combining those transformed variables, we expect that the general solution would take a form $\nu = \nu(\xi)$, or

$$n = t^{-2/(1-\gamma)} \nu(x t^{1/(\gamma-1)}), \tag{20}$$

when $\gamma \neq 1$. This similarity solution obtained from invariant transform is consistent with the result from a more formal analysis by Fournier and Laurençot (2005, 2006b).

Especially, when $\gamma = 0$ and $\gamma = 2$, respectively, the above similarity solution (20) reduces to the form

$$n = \frac{\nu(x/t)}{t^2}, \tag{21a}$$

$$n = t^2 \nu(xt). \tag{21b}$$

Note that $\gamma = 0$ corresponds to the case that the kernel is constant, and $\gamma = 2$ is obtained, for example, from the form, $K = x^2 + y^2$, as qualitatively expected for the cloud droplets (cf., Long, 1974). The first similarity solution (21a) is intuitive to interpret: a peak of the distribution moves towards a larger size linearly with time by keeping its distribution form, associated with a decrease of its peak value proportional to t^{-2}.

On the other hand, the second Eq. (21b) is even unphysical: a peak of distribution moves to a smaller size with t^{-1} associated with the increase of the peak value proportional to t^2. This unphysical nature of the solution can be amended first by realizing the SCE is also invariant by translation in time so that a constant time, t_c, can be subtracted from time in the solution above. Furthermore, re-defining the resulting $\nu(t - t_c)$ as $\nu_1(t_c - t) = \nu(t - t_c)$, and re–setting the latter as $\nu = \nu_1$:

$$n = (t_c - t)^2 \nu(x(t_c - t)). \tag{21c}$$

Here, although the final result may appear to be a consequence of inverting the time direction, the time inversion transformation is actually not applied in the derivation. After this transformation, the peak size of a distribution increases with time, and the maximum decreases with time. However, this solution collapses at a finite time, $t = t_c$, with the peak reaching the infinity. This rather unintuitive result of the collapse of the distribution with a finite time, t_c, is, in fact, consistent with the known tendency of SCE system for gelation with $\gamma > 1$, associated with the loss of mass at infinity (e.g. van Dongen and Ernst, 1988; Escobedo et al., 2002; Leyvraz, 2003; Fournier and Laurençot, 2006b).

Finally, when $\gamma = 1$, from Eq. (18a), we find

$$\xi = t \tag{22a}$$

suggesting that the evolution is primarily controlled by time, t. Combining this conclusion with Eq. (15d) suggests a general solution of the form:

$$n = \nu(t)/x^2. \tag{22b}$$

Note that the solution (22b) already suggests its asymptotic nature: it diverges as $x \to 0$, and the integral of xn diverges as $x \to +\infty$, thus the total mass (Eq. 2) is not well defined: the solution (22b) is valid only over a finite range, say, $[\epsilon, X]$, where ϵ and X are, respectively, a small and large parameters. Yet, this asymptotic behavior is identical to that obtained by van Dongen and Ernst (1988) by a more rigorous analysis.

Substitution of the form (22b) into Eq. (8) further suggests that the problem reduces to the form

$$\frac{d\nu}{dt} = -\nu^2 S, \tag{23a}$$

where S is determined by the integral,

$$S = -\frac{x^2}{2} \int_0^x \frac{K(x-y, y)}{(x-y)^2 y^2} dy + \int_0^{+\infty} \frac{K(x, y)}{y^2} dy. \tag{23b}$$

Since ν is the function of t only, it also follows that S must be a constant. Recall the asymptotic nature of the solution (22b), thus S is also constant only in a certain asymptotic sense.

The differential equation (23a) is readily solved, and we find:

$$\nu = \frac{1}{1/\nu_i + St} \tag{24}$$

with $\nu = \nu_i$ at $t = 0$. The above time dependence is identical to Eq. (C4) in the Appendix C obtained by a separation of variables, but that is also contradicting with the conservation of mass. The fact suggests that the solution (24) is valid only in a limited sense approximately.

The integral of Eq. (23b) can be readily performed, when the kernel, K, is also defined in a simple analytical form. Take for example, the form, $K = x + y$, as suggested by Long (1974) to be appropriate for the rain scale. As a result, the integral (23b) reduces to:

$$S = -\frac{x^3}{2} \int_0^x \frac{1}{(x-y)^2 y^2} dy + \int_0^{+\infty} \left(\frac{1}{y} + \frac{x}{y^2} \right) dy. \tag{25}$$

The two integrals can also be readily performed analytically in indefinite forms and:

$$\int \frac{1}{(x-y)^2 y^2} dy = \frac{2}{x^2(x-y)} - \frac{1}{xy(x-y)} - \frac{2}{x^3} \log \frac{x-y}{y},$$

$$\int \left(\frac{1}{y} + \frac{x}{y^2} \right) dy = -\frac{x}{y} + \log y.$$

However, the integrals become singular with given integral ranges, for the reason already suggested. Thus, we modify the integral ranges to $[\epsilon, x - \epsilon]$ and $[\epsilon, X]$, respectively, assuming ϵ and X be a small and large parameters, respectively. As a result, these two integrals are performed into:

$$\int_\epsilon^{x-\epsilon} \frac{1}{(x-y)^2 y^2} dy = \frac{2}{\epsilon x^2} - \frac{2}{x^3} - \frac{4}{x^3} \log \frac{\epsilon}{x}, \tag{26a}$$

$$\int_\epsilon^X \left(\frac{1}{y} + \frac{x}{y^2} \right) dy = \left(\frac{1}{\epsilon} - \frac{1}{X} \right) x + \log \frac{X}{\epsilon}, \tag{26b}$$

where small contributions due to ϵ are neglected.

The main problem with these results is that direct substitution of them into Eq. (25) does not lead to a result with S a constant, but it depends on x:

$$S = 1 - \frac{x}{X} - 2\log\frac{x}{\epsilon} + \log\frac{X}{\epsilon} = 1 - \frac{x}{X} - 2\log x + \log(\epsilon X).$$

Yet, this merely reflects the asymptotic nature of similarity solutions. Here, the second term drops off with the condition of $x/X \ll 1$. For the x-dependence in the third term also to drop off, and the last term with $\log(\epsilon X)$ to dominate, we further need to assume $\epsilon X \gg 1$ as well as $x \sim 1$. The latter condition ensures that $\log x \sim 1$. Under these conditions, the final result is:

$$S \simeq \log(\epsilon X). \tag{27}$$

Note that this constant can be specified only by specifying the range, $[\epsilon, X]$, over which the asymptotic distribution (22b) is valid.

The extension of the analysis of this section, invoking the Lie algebra–based transformation theory more systematically, is presented in the Appendix D4.

4 Numerical Experiments

In the last section, we have derived the similarity solutions for the SCE by the invariance transformations. In this section, we verify those general invariant solutions (21a), (21c) and (22b) by numerical experiments. In the following, the SCE system is considered in nondimensional units with all the variables also normalized properly. More specifically, all the constants for the kernels, $K(x, y)$, are set to unity, and the mass distributions, $n(x)$, are normalized to unity by integration. Using typical values, $K_0 = 10^{-3}\,\mathrm{cm^3\,s^{-1}}$ and $N_0 = 200\,\mathrm{cm^{-3}}$, we find a typical time scale of the system to be:

$$\tau = 1/K_0 N_0 = 5\,\mathrm{s}.$$

This is the unit of the nondimensional time in the following numerical experiments.

For the purpose of those numerical experiments, we consider three types of idealized kernel forms:

i. $\gamma = 0$: $K(x, y) = 1$.

ii. $\gamma = 1$: $K(x, y) = x + y$.

iii. $\gamma = 2$: $K(x, y) = x^2 + y^2$.

According to Long (1974), the last two forms are conceptually applicable to the rain and cloud droplets, respectively.

The initial mass distribution, n, is the Gamma distribution, as given by:

$$n = \frac{\lambda^{\mu+1}}{\Gamma(\mu+1)} x^{\mu} e^{-\lambda x}, \tag{28a}$$

where λ and μ are the free parameters in the distributions. These parameters are constrained by

$$\lambda = \mu + 1 \tag{28b}$$

due to the normalization condition (6b).

The adopted numerical algorithm is as described in Bott (1998), and we use the code provided by the original author for our computations with minor modifications. The mass range considered for the present study is from $x = 1.2 \times 10^{-9}$ to $x = 1.2 \times 10^{36}$, divided into 300 logarithmically spaced bins. Actual computations are performed over the range where significant values for number density are found, and in the following plots, we will only show a limited range with significant mass densities. The default time step is $\delta t = 0.1$. As detailed in the Appendix E1, the case with $\gamma = 2$ requires a special attention: the upper bound of the computational range is limited to $x = 10^3$ with 80 bins, and a shorter time step with $\delta t = 10^{-7}$ is adopted due to the large values of kernel for large x.

In the following computations, we will find a general tendency of the distribution to approach similarity solutions, as predicted from the invariance analysis in the last section. According to the analysis therein, the distribution should approach a universal form, $\nu(\xi)$, asymptotically as $t \to \infty$. Here, the predicted universal form, $\nu(\xi)$, is obtained by rescalings:

i. For $\gamma = 0$:

$$\nu(\xi) = t^2 n(x, t), \tag{29a}$$
$$\xi = x/t. \tag{29b}$$

ii. For $\gamma = 1$:

$$\nu(\xi) = x^2 n(x, t), \tag{30a}$$
$$\xi = t. \tag{30b}$$

iii. for $\gamma = 2$:

$$\nu(\xi) = n(x, t)/(t_c - t)^2, \tag{31a}$$
$$\xi = x(t_c - t). \tag{31b}$$

Here, a time constant, t_c, suggests a time that the given distribution "collapses".

The following numerical examples are highly selective, but intend to suggest a general behavior for each choice of γ. With each figure for those examples, the top frame (a) is always the distribution, $n(x, t)$, and (b) is the re-scaled universal distribution, $\nu(\xi)$. More quantitative analyses are further presented in the Appendix E2 by invoking the full symmetry analysis presented in the Appendix D.

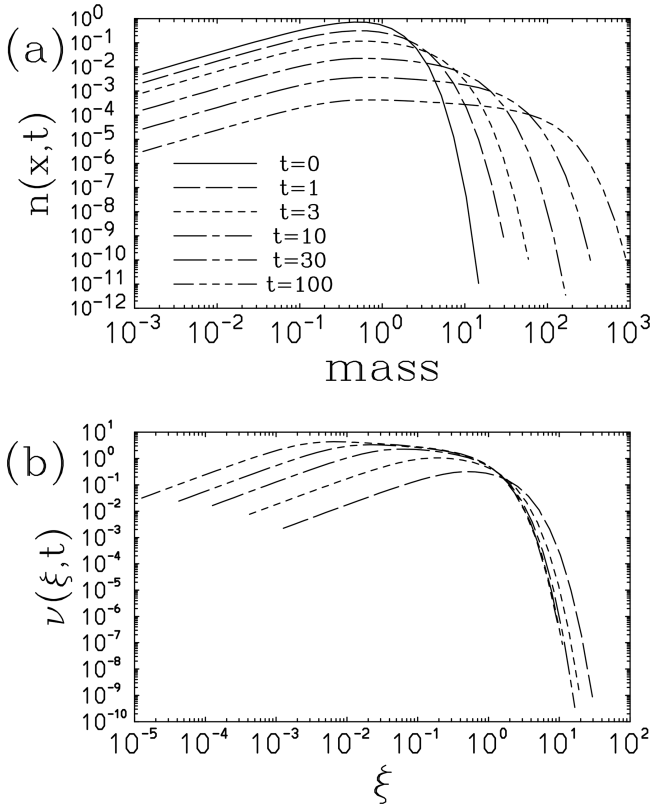

Figure 1. The case with $\gamma = 0$, $K = 1$, initialized by the gamma distribution (Eqs. 28a, 28b) with $\lambda = 2$ and $\mu = 1$: **(a)** The distribution, $n(x,t)$, **(b)** Rescaled distribution, $\nu(\xi,t) = t^2 n(x,t)$: The curves are $t = 0$ (black), $t = 1$ (long dash), $t = 3$ (short dash), $t = 10$ (chain dash), $t = 30$ (double chain dash), and $t = 100$ (triple chain dash). The re-scaled abscissa in **(b)** is defined by $\xi = x/t$.

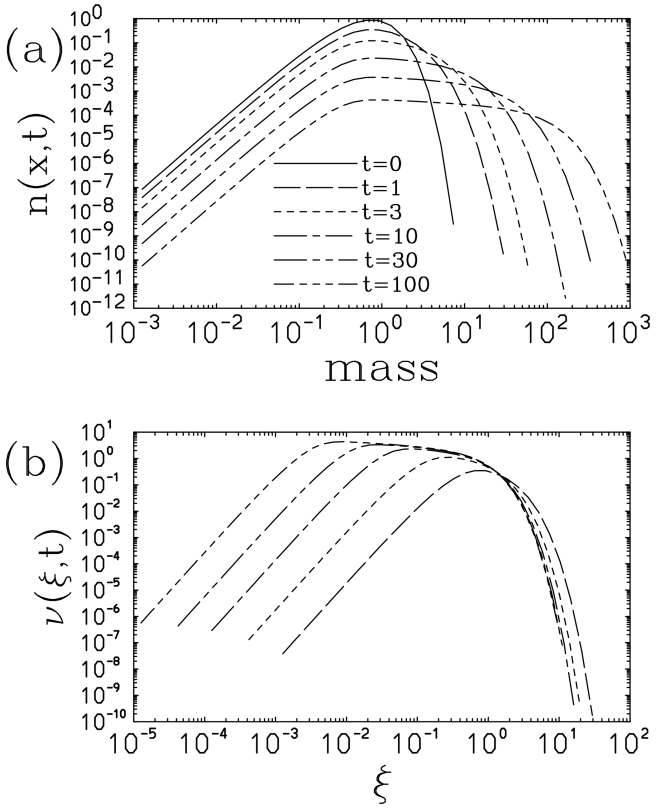

Figure 2. The same as Fig. 1, but with $\lambda = 4$ and $\mu = 3$.

4.1 The Case with $\gamma = 0$:

First to consider is the case with $\gamma = 0$ so that the kernel, K, is a constant, i.e. $K = 1$. The results of numerical time integrations are shown in Figs. 1 and 2, both initialized with gamma distributions.

Figure 1a shows the case initialized with the gamma distribution (Eqs. 28a, 28b) with $\lambda = 2$ and $\mu = 1$: due to the coalescence growth of droplets, the overall distribution evolves to the larger sizes with time with the overall density decreasing, because the coalescence also leads to less number of droplets with time. Figure 1b shows the same, but after rescaling the distribution by Eq. (29a, 29b) into ν as a function of ξ. As time increases, the distribution collapses into a single curve for the larger droplet sizes by $t = 3$, but only gradually with the smaller droplet sizes. However, keep in mind that by taking a logarithmic scale in the horizontal axis, we visualize the relative convergence of the curve, but realize that the absolute difference is almost negligible in the direction of ξ for smaller values.

Figure 2 shows the same, but with $\lambda = 4$ and $\mu = 3$: the initial distribution presents a sharper peak at $x = 1$ as a result. Yet, the overall evolution follows that of Fig. 1: the distribution grows towards the larger masses with time (Fig. 2a) with an overall decrease of the number density. After rescaling (Fig. 2b), the distribution also collapses well for the larger droplet sizes. However, there is no tendency for a collapse seen towards the smaller droplet sizes.

4.2 The Case with $\gamma = 1$:

As a first example of the case with the kernel parameter, $\gamma = 1$, Fig. 3 shows the case initialized by the gamma distribution (Eq. 28a, 28b) with $\lambda = 2$ and $\mu = 1$. As seen in Fig. 3a, in general, the distribution spreads to the larger masses with time, more extensively than the cases with $\gamma = 0$, with the positive tail stretches longer with time.

Note that in this case, the universal function, $\nu(t)$, obtained by multiplying x^2 on the original mass distribution, $n(x,t)$, is expected to become a function of time only (cf., Eqs. 30a, 30b). It follows that, when $\nu(t)$ is plotted as a function of mass, x, as shown in (b), it is expected to becomes a constant. The simulation indeed suggests that the positive tail part approaches a constant with time approximately, albeit with a weak remaining increasing tendency. More precisely, a middle part of the distribution, originating from the point $x = 1$ towards the large x, is close to constant, but weakly increasing, and this range stretches towards the upscale with

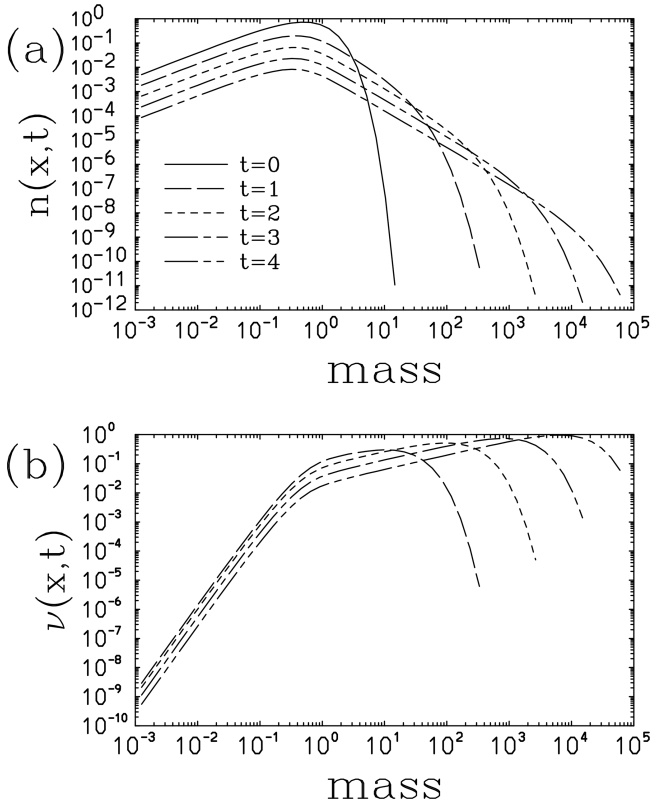

Figure 3. The case with $\gamma = 1$, $K = x+y$, initialized by the gamma distribution (Eqs. 28a, 28b) with $\lambda = 2$ and $\mu = 1$: **(a)** The distribution, $n(x,t)$, **(b)** Rescaled distribution, $v(\xi,t) = x^2 n(x,t)$. The initial distribution ($t = 0$) is in solid curve, with the subsequent evolution marked by varying curves with the curve types defined by insert.

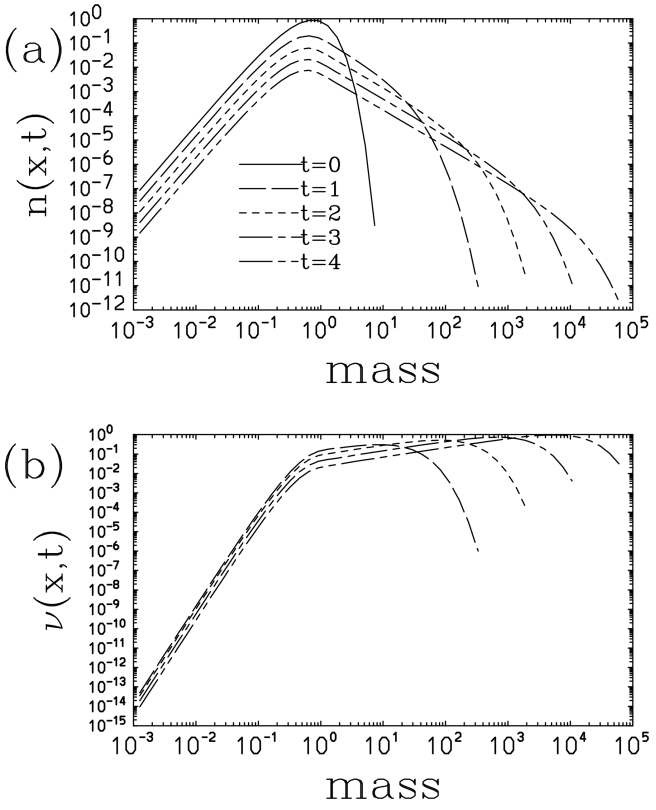

Figure 4. The same as Fig. 3, but with $\lambda = 4$ and $\mu = 3$: **(a)** The distribution, $n(x,t)$, **(b)** Rescaled distribution, $v(\xi,t)$.

time. Also note that the whole distribution represented by the transformed density, $v(t)$, gradually decreases with time, by qualitatively following Eq. (24).

Fig. 4 is the same as Fig. 3, but the increase over the smallest droplet sizes is initially steeper with $\lambda = 3$ and $\mu = 2$, and with a better defined maximum. Nevertheless, the evolution dominated at the larger droplet sizes is very similar to that of Fig. 3. It is shown in the Appendix E2.1 that a remaining weak deviation from the constancy is explained by introducing a more elaborated similarity solution presented in the Appendix D4.5.

4.3 The Case with $\gamma = 2$

With $\gamma = 2$, the asymptotic analysis in Sect. 4 predicts that the distribution collapses at an unspecified time, t_c. However, the numerical results shown in Figs. 5 and 6 simply fail to demonstrate this, due to a very limited upper end for x considered in computations. See the Appendix E2.2 for further discussions on the failure to simulate the collapse.

Instead of collapsing within a finite time, the distribution simply steadily decreases with time. Under these limited numerical computations, the "collapses" is replaced by a tendency that the rules (31a, 31b) transform the distributions at different separate times, $t - t_c$, tend to collapse into a single distribution, as suggested in the frame (b), with $t_c = 2$ both in Figs. 5 and 6. The tendency for this "collapse" is, however, not homogeneous, and the expected overlapping happens more preferably with the smaller mass values.

5 Discussions

The present paper has investigated the stochastic collection equation (SCE) in a standalone manner, when no other physical process contributes, further assuming that collision kernel form does not change by rescaling the droplet size. As a result, SCE becomes scale invariant, i.e. the evolution of the droplet population becomes identical regardless of, say, the initial peak droplet size after a proper rescaling. Conversely, a given droplet population evolution remains a valid solution of the SCE even after any rescaling. An important corollary of this statement is that we do not observe any transformation in the characteristics of the droplet–size distribution as the droplets grow. More specifically, there is no distinction between the cloud and rain droplets arises.

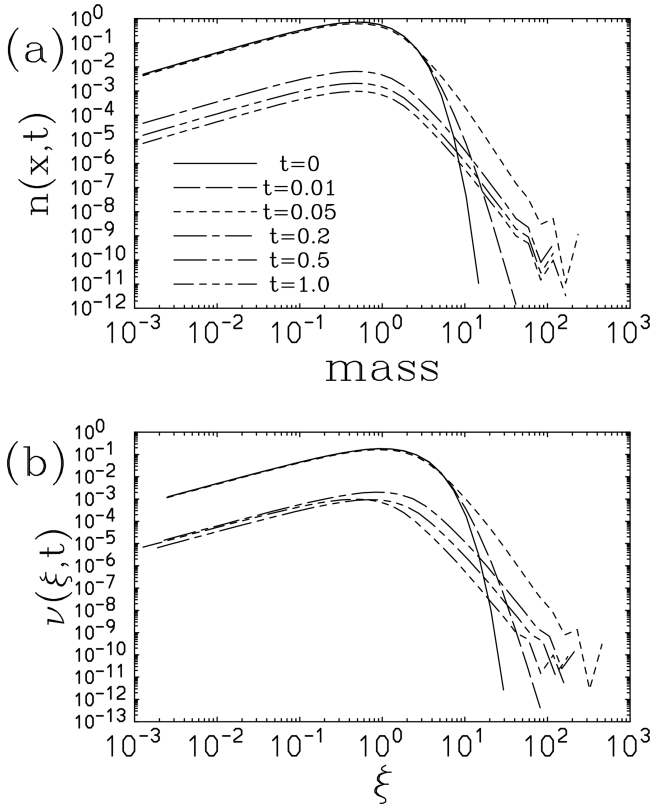

Figure 5. The case with $\gamma = 2$, $K = x^2 + y^2$, initialized by the gamma distribution (Eqs. 28a, 28b) with $\lambda = 2$ and $\mu = 1$: **(a)** The distribution, $n(x,t)$, **(b)** Rescaled distribution, $\nu(\xi,t)$ with $t_c = 2$: the initial distribution ($t = 0$: solid) is followed by $t = 0.01$ (long dash), $t = 0.05$ (short dash), $t = 0.2$ (chain dash), $t = 0.5$ (double chain dash), and $t = 1.0$ (triple chain dash).

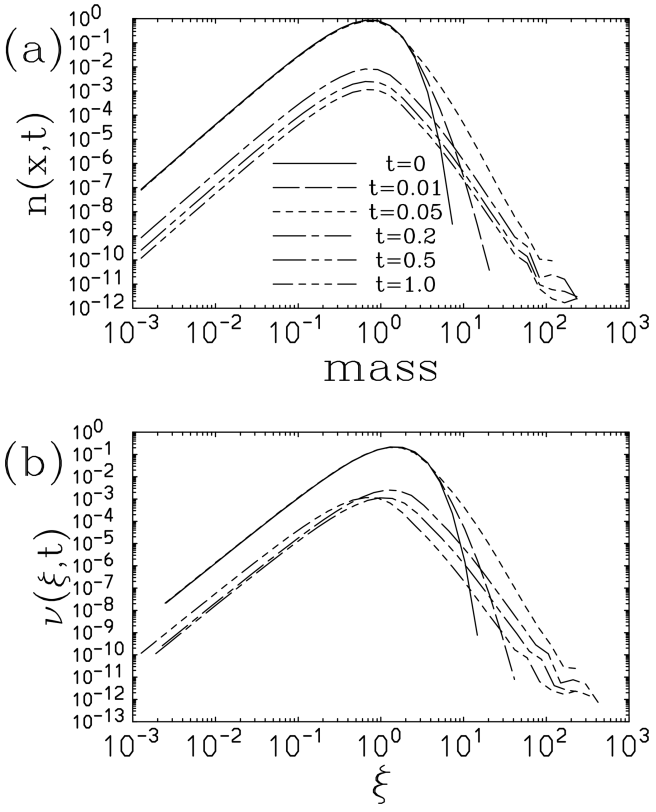

Figure 6. The same as Fig. 5, but with $\lambda = 4$ and $\mu = 3$: **(a)** The distribution, $n(x,t)$; **(b)** Rescaled distribution, $\nu(\xi,t)$ with $t_c = 2$.

Invariant forms derived by invariant transformations in Sect. 3 have been numerically verified in Sect. 4 as asymptotic tendencies towards $t \to +\infty$ with the kernel symmetry with $\gamma = 0$ and 1. Especially, in the case with $\gamma = 1$, the normalized distribution, $\nu = x^2 n$, asymptotically approaches constant with time for the large x, as predicted by the invariant solutions, albeit with a remaining increasing tendency with x: a closer fit is found by considering a more elaborated similarity solution presented in the Appendix D4.5, as shown in the Appendix E2.1.

On the other hand, numerical experiments have failed to reproduce a finite–time collapse predicted by the invariant solution derived with $\gamma = 2$, basically due to a severely limited range of the mass size considered for numerical reasons: only a finite fraction of droplets can be lost at the upper end of the computation domain, simply prolonging the collapse. Yet, we have demonstrated that by the transformations by Eqs. (31a) and (31b), all the later curves tend to collapse into a single curve at small droplet sizes when the critical time, t_c, is taken slightly larger than the maximum time considered.

The most basic conclusion from the present study is that the form of the collection kernel defines the asymptotic tendency of droplet–size distribution. Earlier studies by Berry (1967), and Berry and Reinhardt (1974c, d) suggested that derivatives of the kernel in respect to the droplet sizes define the distribution. According to the present study, it is more precisely, the symmetry characteristics of the kernel in respect to the droplet sizes, that determine the asymptotic tendency of the size distribution with time. Although only the idealized cases are considered in the study, we emphasize the generality of the methodology, which can equally be applied to more realistic settings. Note that in those more realistic applications, the adopted kernels may no longer homogeneous in any strict sense. Thus, the first question to be investigated in degrees that those kernels satisfy the from Eq. (16). More generally, the present study suggests the ways of obtaining physical insights to microphysical problems with more analytically–oriented approaches than currently attempted.

6 From Cloud To Rain

The main body of the present work rather consists of negation: due to the invariance of SCE, when the kernel itself is invariant, we do not observe any characteristic transformation from cloud to rain droplet distributions. An obvious

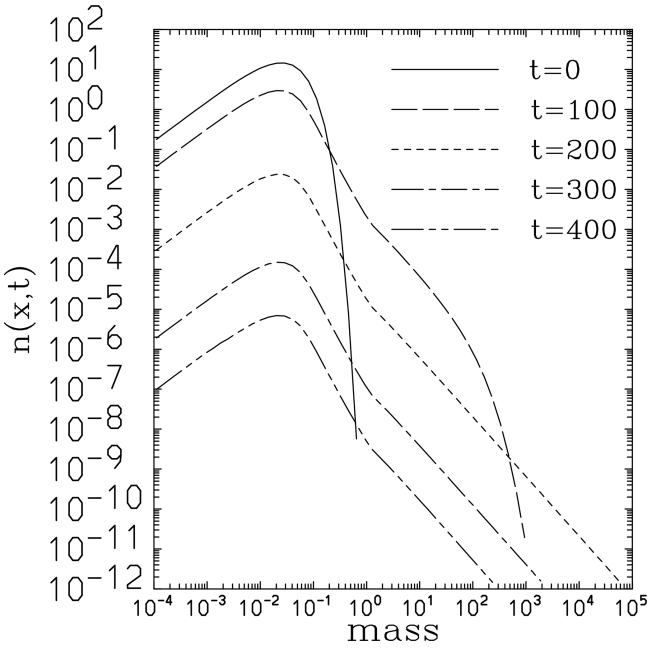

Figure 7. A numerical demonstration of the idealized transition from the cloud to rain state: $\Delta t = 100$.

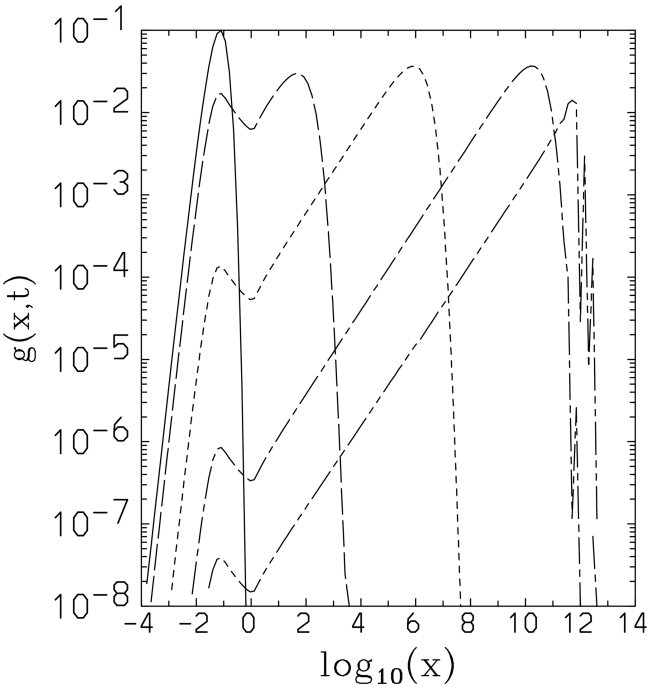

Figure 8. The same as Fig. 7, but showing a transform distribution, $g(x,t)$, defined by Eq. (32), instead of mass distribution, $n(x,t)$. The time interval is $\Delta t = 100$ as before with the same curve types as in Fig. 7.

question to be asked is: would such a transformation from cloud to rain distributions be indeed simulated, when a scale dependence is introduced into the kernel? To respond to this question positively by a numerical demonstration is the purpose of this *post–script* section.

We adopt an idealized kernel introduced by Long (1974):

$$K(x,y) = \begin{cases} x^2 + y^2, & x \le 1 \text{ and } y \le 1, \\ x + y, & \text{otherwise.} \end{cases} \tag{32}$$

Figure 7 is a numerical demonstration of the transition from the cloud to rain: the gamma distribution with $\lambda = 40$ and $\mu = 1$ is assumed as an initial condition. The plot is every $\Delta t = 100$ from $t = 0$: we see that the initial cloud–droplet distribution peaked at $x \simeq 3 \times 10^{-2}$ gradually forms a long tail towards the larger droplet sizes with a clear kink seen at $x = 1$: beyond this scale, the distribution slope becomes distinguishably gentler, marking the rain regime. In interpreting the result here dimensionally, we need to adopt different dimensional scales than in Sect. 4. Here, we re–set: $K_0 = 10^{-3}\,\mathrm{cm^3\,s^{-1}}$ and $N_0 = 10^2\,\mathrm{cm^{-3}}$, thus the characteristic time scale is now about 10 s. Consequently, the cloud droplets grow to the rain droplets taking quarter an hour, reasonably comparable to the observed fast transformation of a cloud into a precipitating mode.

In the literature, a secondary peak marking the rain–droplet contribution is often shown (e.g. Berry and Reinhardt, 1974a, b; Bott, 1998), but this feature is missing from Fig. 7. Here, it is important to realize that in these published plots, rather a transformed distribution, g, defined by

$$g(x,t) = 3x^2 n(x,t) \tag{33}$$

is shown. Although the meaning of this transformed distribution may not be immediately clear, this form is convenient for performing the numerical time integration of the distribution efficiently, as carefully exposed in Bott (1998). One could also consider g to be a measure of mass density in the logarithmic coordinate of mass, because the integral of $g/3$ in respect to $\log x$ leads to the total mass. When this transformed distribution, $g(x,t)$, is plotted, as shown in Fig. 8, we indeed see a formation of a secondary peak for rain.

The reason for identifying the secondary peak by plotting the transformed distribution, $g(x,t)$, is due to the fact that the distribution at the rain scale is characterized by a gentler slope than that over the cloud scale, close to x^{-2} but slightly gentler, as seen in Figs. 3 and 4 with $K = x + y$. This gentle slope leads to a gentle increase with the increasing mass, x, when the transformed distribution, g (Eq. 33), is adopted. Comparing the curve at $t = 100$ between Figs. 8 and 7, one finds that the secondary peak seen in Fig. 8 corresponds to the point that the tendency for the similarity solution is terminated, associated with a sudden drop of distribution. As the range of the similarity solution with $\sim x^{-2}$ evolving upscales, the rain–droplet peak also moves upscales.

Here, importantly, when the gentle slope over the rain regime exactly follows $\sim x^{-2}$ behavior, expected from the

similarity solution, the transformed distribution, g, would be perfectly flat over the rain regime, and then suddenly drops to smaller values beyond the similarity range. Here, a further analysis in the Appendix E2.1 suggests that the rain–distribution slope, more precisely, corresponds to a more elaborated similarity solution presented in the Appendix D4.5 with the slope of $-3/2$. An important corollary from this interpretation is the fact that the similarity solutions presented in Sect. 3 can also be applicable locally: this is an important implication in applying the methodology of the invariant transformations for more realistic settings.

Appendix A: List of Mathematical Notations

A1 Variables

$K(x, y)$	collection kernel, or simply *kernel*, the rate that the two droplets with the masses, x and y, coalescence into the droplet of the mass, $x + y$
N	total droplet number (Eq. 9)
N_0	initial total droplet number (Eq. 5) here the subscript 0 is used by breaking the general rule, because it is also adopted as a nondimensionalization scale of the total droplet number (cf., Eq. 4d)
$\tilde{N}(t)$	time dependence of the number density by separation of variables (Sect. 2.3)
$n(x, t)$	droplet size distribution
$\tilde{n}$	mass dependence of the number density by separation of variables in Sect. 2.3, or dependence on the transformed variable, ξ, in Appendix D4.2
m	total mass of the system (Eq. 3)
S	constant source defined by Eqs. (23b), (D32b)
t	time
t_c	negative constant time for displacement (Eq. 21c), and a critical time for the collapse of distribution
t_0	positive constant time for displacement (Eqs. D21, D27a, D27b).
x	droplet mass
y	(secondary) droplet mass
$\alpha(t)$	stretch rate of the stretched mass coordinate, ξ, defined by Eq. (D26b)
β, β'	constants (Eqs. D47, D48a, D48b, E1)
γ	transformation constant of the kernel by mass, x_0 (Eq. 16)
δt	numerical time step
Δt	increments in time in drawing the curves for the evolution
ξ	transformed variable defined by Eq. (D26b), a stretched mass coordinate
λ	constant parameter of the gamma distribution in Eq. (28a)
ν	normalized mass–distribution density: defined by Eq. (19b) when $\gamma \neq 1$ and by Eq. (22b) when $\gamma = 1$
ξ	(i) when $\gamma \neq 1$, transformed "mass" (Eq. 18b); (ii) when $\gamma = 1$, $\xi = t$, or alternatively $\xi = xe^{-t/t_0}$ (Eqs. D26a, D26b).
χ	constant for the separation of variables (Sect. 2.3, Appendices D4.2, C), which also turns into an eigenvalue of an eigen–equation in each case

A2 Subscripts, Superscrips, and Symbols

$_*$	subscript that donates the dimensional variables
*	superscript that donates the transformed variables (Eqs. 11a–11d)
$\tilde{}$	symbol for indicating the separated dependent variables (Sect. 2.3)
$\bar{}$	Laplace transform
$_0$	subscript that designates the nondimensionalization scales
$_i$	subscript that designates the initial states
$_r$	subscript that designates constants for the transformations (Eqs. 11a–11d)

Appendix B: Mass Conservation of the SCE System

As remarked in association with Eq. (2), the mass conservation of the SCE system is not guaranteed automatically. To address this issue fully, this Appendix derives the mass conservation of SCE in a more explicit manner, and suggests how and when the mass conservation can break down. Here, in this Appendix, we present the equations in *nondimensional form*, dropping the subscript, $*$, suggesting the dimensional variables, because as remarked in the main text, the form of SCE does not change by nondimensionalization,

To address rather subtle mathematical aspects, we examine the budget of the cumulative mass up to the size, X, defined by:

$$m(X) = \int_0^X x n(x,t) \mathrm{d}x. \tag{B1}$$

The total mass defined by Eq. (2) is recovered by taking the limit of $X \to +\infty$. By taking the time derivative of Eq. (B1), we obtain:

$$\frac{\mathrm{d}m(X)}{\mathrm{d}t} = \int_0^X x \frac{\partial n(x,t)}{\partial t} \mathrm{d}x \tag{B2}$$

assuming X is fixed with time.

The budget equation for $m(X)$ is obtained by substituting the right–hand side of Eq. (8) into the integrant on the right–hand side of the equation above. It leads to:

$$\frac{\mathrm{d}m(X)}{\mathrm{d}t} = \frac{1}{2} I_1 - I_2, \tag{B3}$$

where

$$I_1 = \int_0^X \int_0^x x\, n(x-y,t) n(y,t) K(x-y,y) \mathrm{d}y \mathrm{d}x, \tag{B4a}$$

$$I_2 = \int_0^X \int_0^{+\infty} x\, n(x,t) n(y,t) K(x,y) \mathrm{d}y \mathrm{d}x. \tag{B4b}$$

In the integral, I_1, we first reverse the order of integral into $\int_0^X \int_y^X \mathrm{d}x \mathrm{d}y$, then transform the coordinate into $x' = x - y$ from x. As a result we obtain:

$$\begin{aligned} I_1 &= \int_0^X \int_0^{X-y} (x'+y) n(x',t) n(y,t) K(x',y) \mathrm{d}x' \mathrm{d}y \\ &= 2 \int_0^X \int_0^{X-x} x\, n(x,t) n(y,t) K(x,y) \mathrm{d}y \mathrm{d}x, \end{aligned} \tag{B4c}$$

re-arranging the definitions of x' and y for obtaining the second line.

By substituting Eqs. (B4b) and (B4c) into Eq. (B3), the two integral also cancel out except for a residual contribution. Thus:

$$\frac{\mathrm{d}m(X)}{\mathrm{d}t} = -\int_0^X \int_{X-x}^{+\infty} x\, n(x,t) n(y,t) K(x,y) \mathrm{d}y \mathrm{d}x. \tag{B5}$$

Consequently, the mass conservation, $\mathrm{d}m/\mathrm{d}t = 0$, is established, provided that the condition,

$$\lim_{X \to +\infty} \int_0^X \int_{X-x}^{+\infty} x n(x,t) n(y,t) K(x,y) \mathrm{d}y \mathrm{d}x = 0, \tag{B6}$$

is satisfied. That is, when the coalescence growth asymptotically approaches to zero as the droplet size approaches infinity, as also loosely stated by Eq. (3) in the main text.

The tendency with Eq. (B6) may physically be intuitive enough to expect. However, it is not guaranteed mathematically, especially when the kernel, $K(x,y)$, increases unbounded with the increasing, x and y. It can, indeed, mathematically be shown (e.g. van Dongen and Ernst, 1988; Escobedo et al., 2002; Leyvraz, 2003; Fournier and Laurençot, 2006b) that the condition (B6) breaks down when $\gamma > 1$, where γ is an exponent introduced by Eq. (16). In this case, the droplet mass is lost to the infinity by coalescence through the term on the right–hand side of Eq. (B5). This is the basic mechanism of *gelation*.

Appendix C: Solution with the Separation of Variables

The purpose of this Appendix is to present a full analysis for the solution by separation of variables (Eq. 10) introduced in Sect. 2.3.

We introduce the normalization condition

$$\int_0^{+\infty} \tilde{n}(x) \mathrm{d}x = 1, \tag{C1}$$

and $\tilde{N}(t=0) = 1$.

Substituting Eq. (10) into Eq. (8), we obtain

$$\begin{aligned} \tilde{n} \frac{\mathrm{d}\tilde{N}}{\mathrm{d}t} = \tilde{N}^2 \Bigg[&\frac{1}{2} \int_0^x K(x-y,y) \tilde{n}(x-y) \tilde{n}(y) \mathrm{d}y \\ &- \tilde{n}(x) \int_0^{+\infty} K(x,y) \tilde{n}(y) \mathrm{d}y \Bigg], \end{aligned} \tag{C2}$$

thus by introducing a separation constant, χ, we obtain separate equations for time and size dependencies:

$$\frac{\mathrm{d}\tilde{N}}{\mathrm{d}t} = -\chi \tilde{N}^2, \tag{C3a}$$

$$\tilde{n} = -\frac{1}{\chi}\left[\frac{1}{2}\int_0^x K(x-y,y)\tilde{n}(x-y)\tilde{n}(y)\mathrm{d}y - \tilde{n}(x)\int_0^{+\infty} K(x,y)\tilde{n}(y)\mathrm{d}y\right]. \tag{C3b}$$

Equation (C3a) can readily be solved, and:

$$\tilde{N} = \frac{1}{1+\chi t}. \tag{C4}$$

The size distribution, $\tilde{n}$, is also obtained by solving the diagnostic integral equation (C3b) with χ as an eigenvalue of the problem.

However, it is immediately found that this system is not consistent with the mass conservation. First, from the constraint (6b), we find

$$\tilde{N}\int_0^{+\infty} x\tilde{n}(x)\mathrm{d}x = m.$$

Here, we have re-introduced the nondimensional total mass by m, for a clarity of the meaning of the above constraint, though it is unity by definition. From the above, we immediately obtain an expression for the total number, $\tilde{N}(t)$ by

$$\tilde{N}(t) = m\left[\int_0^{+\infty} x\tilde{n}(x)\mathrm{d}x\right]^{-1}. \tag{C5}$$

However, this conclusion leads to a contradiction, because the left-hand side is time dependent, with its solution given by Eq. (C4), whereas the right-hand side is constant in time. Thus, a separable solution is not available for the SCE.

Appendix D: Lie–Algebra Based Symmetry Analysis

Exposition based on a systematic application of the Lie–algebra based symmetry analysis is beyond the scope of the present paper. The first purpose of this Appendix is to present a very basic exposition of this methodology for the interested readers. The further purpose of this Appendix is to present additional technical results, that are of interest to the Lie–algebra specialists, as well as an extension of the analysis of Sect. 3.

D1 Short Introduction

We first present a very succinct and self–contained description of the Lie–algebra based symmetry analysis. Here, we skip all the formal definitions as well as any derivations, even briefly given: the formal mathematical definitions often do not contribute to any sense of understanding for the physicists. The purpose here is to provide the readers with an overview that provides a "feeling" of this methodology. This subsection lists basic formulas used in this mathematical methodology along this line. For fuller expositions, readers are advised to refer to e.g. Bluman and Kumei (1989) and Grigoriev et al. (2010).

The transformations introduced by Eqs. (11a)–(11d) can be written in a more general manner as:

$$x^* = \mathcal{X}(x,t,K,n;a), \tag{D1a}$$
$$t^* = \mathcal{T}(x,t,K,n;a), \tag{D1b}$$
$$K^* = \mathcal{K}(x,t,K,n;a), \tag{D1c}$$
$$n^* = \mathcal{N}(x,t,K,n;a). \tag{D1d}$$

Here, $\mathcal{X}$, $\mathcal{T}$, $\mathcal{K}$, and $\mathcal{N}$ are the transformation functions for x, t, K, and n, respectively, defined as functions of x, t, K, and n and a continuous parameter, a. These transformations satisfy the properties mathematically called *group*. Since these transformations are originally studied by Sophus Lie, thus they are often called the Lie group of transformations. The theory of *group* makes a systematic analysis of the symmetry of the system possible.

As it turns out, the transformations (D1a–D1d) are more conveniently examined in exponential forms given by:

$$x^* = e^{\omega_x(x,t,K,n;a)}x, \tag{D2a}$$
$$t^* = e^{\omega_t(x,t,K,n;a)}t, \tag{D2b}$$
$$K^* = e^{\omega_K(x,t,K,n;a)}K, \tag{D2c}$$
$$n^* = e^{\omega_n(x,t,K,n;a)}n, \tag{D2d}$$

where ω with varying subscripts are the exponents that define the transformations. This point is seen in the following manner: we first define the infinitesimal transformations of Eqs. (D1a)–(D1d) by:

$$x^* = x + a\sigma_x(x,t,K,n), \tag{D3a}$$
$$t^* = t + a\sigma_t(x,t,K,n), \tag{D3b}$$
$$K^* = K + a\sigma_K(x,t,K,n), \tag{D3c}$$
$$n^* = n + a\sigma_n(x,t,K,n). \tag{D3d}$$

setting $a \to 0$ asymptotically. Here,

$$\sigma_x(x,t,K,n) = \frac{\partial\mathcal{X}(x,t,K,n;a)}{\partial a}|_{a=0}, \tag{D4a}$$
$$\sigma_t(x,t,K,n) = \frac{\partial\mathcal{T}(x,t,K,n;a)}{\partial a}|_{a=0}, \tag{D4b}$$
$$\sigma_K(x,t,K,n) = \frac{\partial\mathcal{K}(x,t,K,n;a)}{\partial a}|_{a=0}, \tag{D4c}$$
$$\sigma_n(x,t,K,n) = \frac{\partial\mathcal{N}(x,t,K,n;a)}{\partial a}|_{a=0}. \tag{D4d}$$

Corresponding to those infinitesimal operators, we can introduce the infinitesimal generators by

$$X_x = \sigma_x(x,t,K,n)\frac{\partial}{\partial x}, \tag{D5a}$$

$$X_t = \sigma_t(x,t,K,n)\frac{\partial}{\partial t}, \tag{D5b}$$

$$X_K = \sigma_K(x,t,K,n)\frac{\partial}{\partial K}, \tag{D5c}$$

$$X_n = \sigma_n(x,t,K,n)\frac{\partial}{\partial n}. \tag{D5d}$$

As a result, the exponential transformations are represented in terms of those infinitesimal operators by

$$\omega_x = aX_x, \tag{D6a}$$

$$\omega_t = aX_t, \tag{D6b}$$

$$\omega_K = aX_K, \tag{D6c}$$

$$\omega_n = aX_n \tag{D6d}$$

with a minor translations that those exponents, ω, with varying subscripts, also becomes operators. However, operating on the variables, x, t, K, and n to the front, we recover the identical transformations. Here, the algebra based on the infinitesimal operators, Eqs. (D5a)–(D5d), is called the Lie algebra.

By combining them together, the whole system can be transformed by a generator,

$$X = X_x + X_t + X_K + X_n. \tag{D7}$$

By using this generator, the transformations, that makes any differential equation, symbolically written as,

$$\Phi(x,t,K,n) = 0, \tag{D8}$$

to be invariant, are obtained by the condition,

$$X\Phi\Big|_{\Phi=0} = 0. \tag{D9}$$

In other words, by solving the differential equation system defined by Eq. (D9), we can obtain invariant transformations of the system (Eq. D8) by solving for the parameters, σ_x, σ_t, σ_K, and σ_n. The solution of the operator, X, that satisfies Eq. (D9) is usually not unique, and the obtained solution forms a *group* of transformations. Thus, we designate this set of transformations by X_j with the subscript spanning for $j = 1, 2, \ldots, n_t$, where n_t is the total number of invariant transformations identified. Application of the methodology to integro-differential equations requires transformation of the operator (D9) to its generalised canonical form, as described by Grigoriev et al. (2010). The central idea is that the generalised canonical form of the operator, when applied to Eq. (D8), does not act on the independent variables. Hence, it also nicely circumvents the problem of treating integrals and their boundaries: see also Wacławczyk et al. (2017).

An important operator to consider is:

$$[X_i, X_j] = X_iX_j - X_jX_i, \tag{D10a}$$

called the commutator, defined in terms of any two generators, X_i and X_j. A theorem says that if the two generators, X_i and X_j, constitute invariant transformations, another generator, X_k, arising from the commutator,

$$[X_i, X_j] = X_k, \tag{D10b}$$

also constitutes an invariant transformation. This theorem is useful to verify whether we have indeed obtained a full set of invariant transformations by solving Eq. (D9).

Finally, by using those obtained invariant transformations, the invariant relations as given by e.g. Eq. (15e) in the main text is obtained by solving the characteristic equation,

$$\frac{\mathrm{d}x}{\sigma_x} = \frac{\mathrm{d}t}{\sigma_t} = \frac{\mathrm{d}K}{\sigma_K} = \frac{\mathrm{d}n}{\sigma_n}. \tag{D11}$$

D2 Invariant transformations of SCE

The invariant transformations of SCE identified in the main text can be re–cast into the framework of the Lie–group transformation introduced in the last section. The most general invariant scaling transformation (13a), identified in the main text, is expressed in terms of the exponential form (D2a–D2d) as:

$$\omega_x + \omega_t + \omega_K + \omega_n = 0. \tag{D12}$$

Here, there are the four parameters, ω_x, ω_t, ω_K, and ω_n, constrained by a single condition (D12). Thus, three of those four parameters can be changed freely, still satisfying the invariant transformation condition (D12). In this manner, retaining only two of the four parameters in Eq. (D12), for example, we obtain the following three invariant conditions:

$$\omega_x + \omega_K = 0, \tag{D13a}$$

$$\omega_t + \omega_n = 0, \tag{D13b}$$

$$\omega_K + \omega_n = 0. \tag{D13c}$$

With the help of the relations (D6a–D6d) as well as the definitions of the individual generators, Eqs. (D5a)–(D5d), and substituting them into Eq. (D7), we obtain the three corresponding generators,

$$X_1^G = x\partial_x - K\partial_K, \tag{D14a}$$

$$X_2^G = t\partial_t - n\partial_n, \tag{D14b}$$

$$X_3^G = K\partial_K - n\partial_n. \tag{D14c}$$

Here, the superscript, G, has been added to distinguish them from different sets of operators introduced later. Different superscripts will be added to the other operators introduced subsequently for distinction, but without further remarks.

From these three generators, the three characteristic equations, as defined by Eq. (D11), can be introduced:

$$\frac{\mathrm{d}x}{x}+\frac{\mathrm{d}K}{K}=0, \tag{D15a}$$

$$\frac{\mathrm{d}t}{t}+\frac{\mathrm{d}n}{n}=0, \tag{D15b}$$

$$\frac{\mathrm{d}K}{K}+\frac{\mathrm{d}n}{n}=0, \tag{D15c}$$

and solving them, we obtain the following invariance relations:

$$xK=\text{const.}, \tag{D16a}$$

$$nt=\text{const.}, \tag{D16b}$$

$$nK=\text{const.} \tag{D16c}$$

The invariance relation (D16b) corresponds to Eq. (14a) in the main text.

By using the commutator, Eq. (D10a), we can verify whether the three generators, Eqs. (D15a)–(D15c) constitute a closed set. As it turns out, all those three generators are commutable without generating a new generator. Note that there are more possible combinations among the four parameters to form two–parameter constraints. However, those generators defined from those combinations can be expressed by the three generators already defined by Eqs. (D14a)–(D14c). Namely, $X_1^G+X_3^G=x\partial_x-n\partial_n$, $X_2^G-X_3^G=t\partial_t-K\partial_K$, and $X_1^G-X_2^G+X_3^G=x\partial_x-t\partial_t$.

As pointed out in the main text, the most general invariant transformation (D12) is not complete, but further constrained. First, the total mass must be conserved, which leads to a constraint of Eq. (15c). It can be alternatively stated in terms of the exponent parameters as

$$2\omega_x+\omega_n=0. \tag{D17a}$$

Furthermore, the kernel, K, is constrained by Eq. (16), which is equivalently stated as

$$\omega_K=\gamma\omega_x. \tag{D17b}$$

By using those two constraints, (D17a, D17c), the general scaling invariance relation (D12) reduces to:

$$(-1+\gamma)\omega_x+\omega_t=0. \tag{D17c}$$

By translating the constraints, Eqs. (D17a) and (D17b), into the characteristic equations, from there we obtain the well–constrained generator as

$$X^{\mathrm{C}}=x\partial_x+(1-\gamma)t\partial_t-2n\partial_n. \tag{D18}$$

D3 Formal Application of the Lie Transformation Group to SCE

Obtaining general invariant transformation relations formally from Eq. (D9) is lengthy and tedious. Yet, it is done by Lin et al. (2024), and they present the following set of invariant transformations (their Eq. 2.54):

$$X_1^L=x\partial_x-(1+\gamma)t\partial_t, \tag{D19a}$$

$$X_2^L=t\partial_t-n\partial_n, \tag{D19b}$$

$$X_3^L=\partial_t. \tag{D19c}$$

The second generator, X_2^L, corresponds to X_2^G, identified in the last section by Eq. (D14b). However, the remaining two do not directly correspond to any generators identified in the last section.

The first two generators are best understood as a consequence of only introducing the constraint on the kernel (Eq. D17b) to the general constraint given by Eq. (D12). By directly substituting Eq. (D17b) into Eq. (D12), we obtain

$$(1+\gamma)\omega_x+\omega_t+\omega_n=0. \tag{D20}$$

By setting $\omega_n=0$ or $\omega_x=0$, respectively, in the above, we recover the first two generators, Eqs. (D19a) and (D19b).

By recovering their first two generators in this manner, it also transpires that the Lie–algebra analysis presented by Lin et al. (2024) do not take the mass conservation constraint, Eq. (D17a) into account. Under this constraint, the two generators, X_1^L and X_2^L, are no longer independent, but it can only be used with a linear combination of $X_1^L+2X_2^L$. That is the generator obtained as Eq. (D18) in the last subsection.

On the other hand, the generator, X_3^L, is new here: a simple inspection tells us that it corresponds to the time translation invoked in deriving Eq. (21c). Possibility of time–translation invariance has been excluded in simple invariant transformations (Eqs. 11a–11d) considered in the main text. It is the advantage of the analysis by the Lie transformation group that can lead to an exhaustive list of transformations. However, also note that the time–translation invariance itself can be verified from a given integro–differential equation by a conventional method easily.

In summary, the SCE system remains invariant under two transformations, given by Eqs. (D18) and (D19c). Thus, by introducing an arbitrary constant, t_0, the general generator for the invariant transformation for SCE is given by

$$X=x\partial_x+[(1-\gamma)t+t_0]\partial_t-2n\partial_n. \tag{D21}$$

Finally, one may wish to know the commutation relation between between X^{C} (Eq. D18) and the time–translation, ∂_t, as given by Eq. (D19c). Here, we find:

$$[X^{\mathrm{C}},\partial_t]=-(1-\gamma)\partial_t. \tag{D22}$$

D4 Extension of the Analysis of Sect. 3

D4.1 Alternative Invariant Form with $\gamma=1$

The general transformation rule given by Eq. (D21) not only recovers all the similarity solutions identified in the main

text, but it also leads to more extensive possibilities. A notable example is obtained by setting $\gamma = 1$ in Eq. (D21), which leads to the two characteristic equations:

$$\frac{\mathrm{d}t}{t_0} = \frac{\mathrm{d}x}{x}, \tag{D23a}$$

$$\frac{\mathrm{d}t}{t_0} + \frac{\mathrm{d}n}{2n} = 0, \tag{D23b}$$

Solving them, we identify the two transformed variables

$$\xi = xe^{-t/t_0}, \tag{D24a}$$

$$\nu = ne^{2t/t_0}, \tag{D24b}$$

suggesting a similarity solution of the form,

$$n = e^{-2t/t_0}\nu(xe^{-t/t_0}). \tag{D25}$$

This solution may be compared with the solution by Golovin (1963) and Scott (1968), as discussed further below.

D4.2 Invariant Solutions of SCE

In Sect. 3, invariant forms (20) and (21c) have been inferred directly by identifying the invariant transformations arising from the symmetries of the governing stochastic collection equation (SCE). Here, we seek invariant solutions by substituting these forms back into the SCE. In symmetry analysis, this procedure leads to a reduction of the governing equation to a form that is easier to solve analytically or numerically (e.g. reducing a partial differential equation to an ordinary differential equation; Grigoriev et al. (2010). In the present context, this procedure may also be regarded as a direct extension of the separation of variables examined in the Appendix C.

A starting point is to realize that similarity solutions obtained both by Eqs. (20) and (D25) take a general form

$$n(x,t) = \tilde{N}(t)\tilde{n}(\xi), \tag{D26a}$$

where, ξ is a transformed mass, as defined by Eqs. (18b) and (D24a). Note further that both transformed masses take the form,

$$\xi = \alpha(t)x, \tag{D26b}$$

where $\alpha(t)$ is defined for $\gamma \neq 1$ and $\gamma = 1$, respectively, by

$$\alpha(t) = (1 + t/t_0)^{1/(\gamma-1)}, \tag{D27a}$$

$$\alpha(t) = \mathrm{e}^{-t/t_0} \tag{D27b}$$

in Eqs. (19b) and (D24a), also adding a freedom for a translation, t_0 in Eq. (D27a). Note also that both are normalized to satisfy the condition, $\alpha(0) = 1$ for the later purpose. The form (D26b) is originally proposed by Friedlander (1961), further pursued by e.g. Scott (1968) and Drake (1972), and reviewed in Sects. 11.7.2 and 15.3.2 of Pruppacher and Klett (1997).

To further develop this generalized separation of variables, we first recall the normalization conditions, Eqs. (4a) and (4b). In the same manner, we introduce the normalization conditions as:

$$\int_0^{+\infty} \tilde{n}(\xi)\mathrm{d}\xi = 1, \tag{D28a}$$

$$\int_0^{+\infty} \xi\tilde{n}(\xi)\mathrm{d}\xi = 1. \tag{D28b}$$

These two constraints lead to the two relations for $\tilde{N}$ and α:

$$\tilde{N} = \alpha N, \tag{D29a}$$

$$\alpha^2 = \tilde{N}, \tag{D29b}$$

where N is the total number density (Eq. 9). As a result, we find that both $\tilde{N}$ and α are determined from the total number density, N, by

$$\tilde{N} = \alpha^2, \tag{D30a}$$

$$\alpha = N. \tag{D30b}$$

Here, these relations are obtained by simply substituting the forms (D26a, D26b) into the constraints (D28a, D28b). Alternatively, the same can be obtained by re-writing those constraints in terms of the exponential parameters, then the same conclusions follow as the invariant conditions.

From Eqs. (D26a) and (D26b), respectively, the following two relations are immediately identified:

$$\frac{\partial n}{\partial t} = \tilde{n}\frac{\partial \tilde{N}}{\partial t} + \left(\xi\frac{\partial \tilde{n}}{\partial \xi}\right)\frac{\dot{\alpha}}{\alpha}\tilde{N}, \tag{D31a}$$

$$K(x,y) = K(\xi/\alpha, \eta/\alpha) = \alpha^{-\gamma}K(\xi,\eta), \tag{D31b}$$

setting $\eta = \alpha y$ and recalling the relation (16). Equation (D31a) further reduces to:

$$\frac{\partial n}{\partial t} = \dot{\alpha}\alpha\left(2\tilde{n} + \xi\frac{\mathrm{d}\tilde{n}}{\mathrm{d}\xi}\right), \tag{D31c}$$

with a help of Eq. (D30a).

Under the transformations given by Eqs. (D26a) and, (D26b), with the help of Eqs. (D31a) and (D31b), SCE (Eq. 8) reduces to:

$$\left(2\tilde{n} + \xi\frac{\partial \tilde{n}}{\partial \xi}\right)\dot{N} = N^{-\gamma+2}S(\xi), \tag{D32a}$$

where

$$S(\xi) = \frac{1}{2}\int_0^{\xi} \tilde{n}(\xi-\eta)\tilde{n}(\eta)K(\xi-\eta,\eta)\mathrm{d}\eta - \tilde{n}(\xi)\int_0^{+\infty} \tilde{n}(\eta)K(\xi,\eta)\mathrm{d}\eta \tag{D32b}$$

plays a role of the source term in Eq. (D32a). Note that Eq. (D32a) is equivalent to Eq. (5) of Xie (2024).

Equation (D32a) is separated into the two equations by introducing a separation constant, χ:

$$\dot{N} = -\chi N^{-\gamma+2}, \tag{D33a}$$

$$2\tilde{n}+\xi\frac{\partial\tilde{n}}{\partial\xi} = -\frac{1}{\chi}S(\xi). \tag{D33b}$$

Here, Eq. (D33b) constitutes a nonlinear eigenvalue problem to be solved for $\tilde{n}$ and χ subject to Eqs. (D28a) and (D28b). The eigenvalue, χ, can be, determined from the normalization conditions, (D28a), (D28b):

$$\chi = \frac{1}{2}\int_0^{+\infty}\int_0^{+\infty} K(\xi,\eta)\tilde{n}(\xi)\tilde{n}(\eta)\mathrm{d}\xi\mathrm{d}\eta. \tag{D34}$$

More specifically, it is obtained by directly integrating Eq. (D33b) over ξ. This, in turn, becomes a constraint in solving Eq. (D33b).

The time dependence of the system is also obtained immediately by solving Eq. (D33a) and we recover Eqs. (D27a) and (D27b) with

$$\chi = \frac{1}{t_0(1-\gamma)}, \tag{D35a}$$

$$\chi = 1/t_0, \tag{D35b}$$

respectively, for $\gamma\neq 1$ and $\gamma = 1$. Conversely, we can directly reduce Eq. (D31c) by invoking Eqs. (D27a) and (D27b), and obtain:

$$\frac{1}{t_0(\gamma-1)}\left(2\tilde{n}+\xi\frac{\mathrm{d}\tilde{n}}{\mathrm{d}\xi}\right) = S(\xi), \tag{D36a}$$

$$-\frac{1}{t_0}\left(2\tilde{n}+\xi\frac{\mathrm{d}\tilde{n}}{\mathrm{d}\xi}\right) = S(\xi), \tag{D36b}$$

respectively, for $\gamma\neq 1$ and $\gamma = 1$. Equations (D36a) and (D36b) is equivalent to Eq. (D33b) through the relations (D35a) and (D35b). In the following, we consider solutions with the two special forms of kernel with $\gamma = 0$ and 1.

D4.3 When the kernel is constant

Let $\gamma = 0$ and $K = 1$, then Eqs. (D34) and (D35a) lead to $\chi = 1/2$ and $t_0 = 2$. The source term defined by Eq. (D32b) reduces to:

$$S = \frac{1}{2}\int_0^{\xi}\tilde{n}(\xi-\eta)\tilde{n}(\eta)\mathrm{d}\eta - \tilde{n}(\xi). \tag{D37}$$

We solve Eq. (D33b) by Laplace transformation, designating it as $\mathcal{L}$, which is defined for any function, $f(\xi)$, as:

$$\bar{f}(p) = \mathcal{L}[f] = \int_0^{+\infty} f(\xi)e^{-p\xi}\mathrm{d}\xi, \tag{D38}$$

where $\bar{f}(p)$ is the Laplace transform. First, applying the Laplace transform, $\bar{S}$, to Eq. (D37),

$$\bar{S} = \int_0^{+\infty} Se^{-p\xi}\mathrm{d}\xi = \frac{\bar{n}^2}{2} - \bar{n}, \tag{D39a}$$

invoking a well known formula for the Laplace transform of a convolution,

$$\mathcal{L}[\int_0^{\xi} f(\xi-\eta)g(\eta)\mathrm{d}\eta] = \bar{f}\bar{g}, \tag{D39b}$$

for any arbitrary functions, f and g.

In performing the Laplace transform on the left-hand side of Eq. (D33b), we note another formula:

$$\frac{\partial\bar{f}}{\partial p} = -\int_0^{+\infty}\xi f e^{-p\xi}\mathrm{d}\xi. \tag{D40a}$$

By performing an integral by part, and applying the above formula (D40a),

$$\int_0^{+\infty}\xi\frac{\partial\tilde{n}}{\partial\xi}e^{-p\xi}\mathrm{d}\xi = -\int_0^{+\infty}(1-p\xi)\tilde{n}e^{-p\xi}\mathrm{d}\xi$$
$$= -(\bar{n}+p\frac{\partial\bar{n}}{\partial p}). \tag{D40b}$$

With the help of the result (D40b), we obtain

$$\mathcal{L}\left[2\tilde{n}+\xi\frac{\partial\tilde{n}}{\partial\xi}\right] = \bar{n} - p\frac{\mathrm{d}\bar{n}}{\mathrm{d}p}. \tag{D40c}$$

By referring to Eqs. (D39a) and (D40c), we find that the Laplace transform of Eq. (D33b) is:

$$\frac{\partial}{\partial p}(p\bar{n}) = \bar{n}^2, \tag{D41a}$$

which leads to a solution, $\bar{n} = \beta/(p+\beta)$, with β a constant. After inverse transform, we find :

$$\tilde{n} = e^{-\xi}, \tag{D41b}$$

where $\beta = 1$ by the normalization condition (D28a).

By putting Eqs. (D26a), (D26b), (D27a), and (D41b) together,

$$n = \frac{e^{-x/(1+t/2)}}{(1+t/2)^2}. \tag{D42}$$

This solution is originally obtained by Schumann (1940) and reproduced in Sect. 11.7.2 of Pruppacher and Klett (1997). Note also that with $t\to\infty$, the above solution asymptotically approaches to the invariant solution (21a) with $\nu(\xi) = e^{-2\xi}$. Here, $x/(1+t/2)\to 2x/t$ as $t\to\infty$, and recall that $\xi = x/t$. Moreover, Menon and Pego (2004) show that the tendency to $\nu(\xi)\to e^{-2\xi}$ is a unique asymptotic tendency.

D4.4 When $\gamma = 1$: Standard Similarity Solutions

Letting $K = x + y$, Eqs. (D34) and (D35b) lead to $\chi = 1$ and $t_0 = 1$, and the source term defined by Eq. (D32b) reduces to:

$$S = \frac{\xi}{2}\int_0^{\xi} \tilde{n}(\xi-\eta)\tilde{n}(\eta)\mathrm{d}\eta - (1+\xi)\tilde{n}(\xi). \tag{D43a}$$

The Laplace transform of the above is, again, using Eqs. (D39b) and (D40a):

$$\bar{S} = -\frac{1}{2}\frac{\mathrm{d}\bar{n}^2}{\mathrm{d}p} + \frac{\mathrm{d}\bar{n}}{\mathrm{d}p} - \bar{n}. \tag{D43b}$$

Thus, Eq. (D33b) reduces by Laplace transform to:

$$\bar{n} - p\frac{\mathrm{d}\bar{n}}{\mathrm{d}p} = \frac{1}{2}\frac{\mathrm{d}\bar{n}^2}{\mathrm{d}p} - \frac{\mathrm{d}\bar{n}}{\mathrm{d}p} + \bar{n}, \tag{D43c}$$

or

$$(\bar{n} + p - 1)\frac{\mathrm{d}\bar{n}}{\mathrm{d}p} = 0. \tag{D43d}$$

It gives the two possible solutions, $\mathrm{d}\bar{n}/\mathrm{d}p = 0$ and $\bar{n} = 1 - p$. However, both solutions can be refused based on their unphysical nature.

(i) When $\mathrm{d}\bar{n}/\mathrm{d}p = 0$: $\bar{n}$ is a constant in this case, and its inverse transform leads to $\tilde{n}(\xi) = \delta(\xi)$, taking into account the normalization condition. Substituting $\xi = xe^{-t}$ to this solution, we find $\tilde{n} = e^t\delta(x)$. Combining it with Eq. (D26a), the full solution is:

$$n = \delta(x) \tag{D43e}$$

i.e. all the droplets just stay at the state of the zero size: it is not physically meaningful. It does not satisfy the mass conservation (6b), either.

(ii) When $\bar{n} = 1 - p$: this does not have any physically meaningful solution, either. It can be shown in the following manner. Recall that the Laplace transform is defined by Eq. (D38). Thus, when f is positive definite, since the whole integrant for the transform is positive, the resulting transform, $\bar{f}$, must be positive definite. Conversely, when $\bar{f}$ is negative somewhere, f must be negative somewhere. Thus, $\bar{n}$, which becomes negative at certain values of p cannot be consistent with the positive definite nature of the number density, n. Consequently, this solution is unphysical, too. Lack of physical solution of the form (D26a), (D26b) reflects a known singular behavior of the system with $\gamma = 1$ as discussed in e.g. Sect. 6 of van Dongen and Ernst (1988).

D4.5 When $\gamma = 1$: Alternative Solution

When $\gamma = 1$, alternative solution becomes possible, as already shown in Sect. D4.1. However, this solution is missing from the analysis in the last subsection. The purpose of this subsection is to re–derive it under the framework of this section. For this purpose, we first need to note a mathematically known fact (van Dongen and Ernst, 1988) that the solution with $\gamma = 1$ tends to be singular as $x \to 0$, also suggested by the simplest similarity solution (22b). Thus, for constructing an asymptotic solution, we focus on the limit of $x \to +\infty$. The main consequence by limiting the validity range of a solution is that the given solution no longer satisfies the mass conservation. As a result, those solutions can no longer be constrained by the conditions (D28a), (D28b), and it also follows that they no longer satisfy Eq. (D34). Consequently, the eigenvalue, χ is left undetermined.

Furthermore, the singularity as $x \to 0$, suggests that the number density, n, tends to be concentrated towards $x \to 0$, and the contribution of the droplet number towards the limit of $x \to +\infty$ tends to be negligible. Consequently, we can drop the contribution of the term, $\int_0^{+\infty}\tilde{n}(\eta)\mathrm{d}\eta$, in the source term (D32b) written for the linear kernel $K(\xi,\eta) = \xi + \eta$. As a result, the Laplace transform (D43a) reduces in place of Eq. (D43b) to:

$$\bar{S} = -\frac{1}{2}\frac{\mathrm{d}\bar{n^2}}{\mathrm{d}p} - \bar{n}, \tag{D44}$$

and Eq. (D33b) reduces to:

$$(\bar{n} + \chi p)\frac{\mathrm{d}\bar{n}}{\mathrm{d}p} - (\chi - 1)\bar{n} = 0. \tag{D45a}$$

The above can be solved implicitly as:

$$p(\bar{n}) = -\bar{n} + \beta\bar{n}^{1/(1-t_0)}, \tag{D45b}$$

where β is a constant and $t_0 = 1/\chi$, as follows from relation (D35b). When we set $t_0 = 1/2$, Eq. (D45b), can be solved explicitly for $\bar{n}$:

$$\bar{n}(p) = \frac{1 - \sqrt{4\beta p + 1}}{2\beta}. \tag{D45c}$$

Its inverse Laplace transform is :

$$\tilde{n}(\xi) = \frac{1}{2\beta}\delta(\xi) + \frac{1}{2\sqrt{\beta\pi}}\xi^{-3/2}e^{-\xi/4\beta}. \tag{D46}$$

Here, the first term with the Dirac delta $\delta(\xi)$ does not contribute in the asymptotic limit of $\xi \to +\infty$ that we seek, thus can be dropped. Thus,

$$\tilde{n}(\xi) = \frac{1}{2\sqrt{\beta\pi}}\xi^{-3/2}e^{-\xi/4\beta}. \tag{D47}$$

Finally, substituting the solution (D47) into Eq. (D26a), also with a help of Eq. (D30b), the number concentration $n(x,t)$ reads:

$$n(x,t) = \frac{1}{2\sqrt{\beta\pi}}\xi^{-3/2}\exp\left[-\frac{\xi}{4\beta} - t\right],$$

Alternatively, it reads:

$$n(x,t) = \frac{x^{-3/2}}{2\sqrt{\beta\pi}} \exp\left[-\frac{x}{4\beta}e^{-2t} - t\right]. \tag{D48a}$$

Furthermore, by taking the asymptotic limit of $t \to +\infty$, the solution (D48a) tends to:

$$n(x,t) \to \frac{x^{-3/2}}{2\sqrt{\beta\pi}} e^{-t} \tag{D48b}$$

On the other hand, with a help of an additional transformation of time given by

$$\tau = 1 - N(t), \tag{D49a}$$

an exact analytical solution is obtained (e.g. Golovin, 1963; Scott, 1968)

$$n(x,t) = \frac{(1-\tau)e^{-(1+\tau)x}}{x\sqrt{\tau}} I_1(2x\sqrt{\tau}), \tag{D49b}$$

where $\tau = 1 - e^{-t}$, and I_1 is the first-order modified Bessel function of the first kind. Note that van Dongen and Ernst (1988), Grigoriev and Meleshko (1995), as well as Sect. 11.3.2 of Pruppacher and Klett (1997) further show that how general invariant solutions for SCE is obtained by exploiting the transformation (D49a) systematically. See Grigoriev et al. (2010) for more general discussions.

Although Eq. (D49b) is not in the invariant form (D26a), (D26b), it can be shown that it also tends to be Eq. (D48b) as $t \to +\infty$ in the following manner: after re-setting to $1 - \tau = e^{-t}$, the remaining contribution becomes $\tau \to 1$. Especially, $2x\sqrt{\tau} \to 2x$. Next note an asymptotic tendency of the modified Bessel function:

$$I_1(z) \to \frac{e^z}{\sqrt{2\pi z}}. \tag{D50a}$$

Substituting all those asymptotic tendencies into Eq. (D49b), we find:

$$n(x,t) \to \frac{e^{-t}e^{-2x}}{x} \frac{e^{2x}}{2\sqrt{\pi x}} \tag{D50b}$$

or

$$n(x,t) \to \frac{1}{2\sqrt{\pi}} x^{-3/2} e^{-t}, \tag{D50c}$$

which is equivalent to Eq. (D48b), when we set $\beta = 1$.

Appendix E: Further on Numerical Experiments

The purpose of this Appendix is to further discuss some numerical issues as well as further numerical analyses on the numerical experiments presented in Sect. 4 of the main text.

E1 Numerical Issues: Time Stepping

Extensive test of the code adopted in the present study is already performed in the original paper by Bott (1998). Our further testing simply proves how robustly the code was constructed: the result changes hardly by reducing the time step by factor of ten or reducing the mass grid increment rate. In some cases, the time step has been reduced by several orders of magnitudes, but without showing any sensitivity.

Here, the main numerical issue is a drastic increase of the mass transfer rate with increasing droplet sizes when $\gamma \geq 1$. When $\gamma = 1$, since the distribution decays fast enough with increasing droplet sizes, this does not become an issue in practice, and the experiment can be performed with the standard time step of $\delta t = 0.1$. To ensure this conclusion, the time step has been even decreased to $\delta t = 10^{-4}$, as a comparable procedure as the case with $\gamma = 2$ below, but no change in the results is found.

On the other hand, we face a real numerical difficulty for running the case with $\gamma = 2$ due to the fact that the kernel goes up very fast with increasing x and y with the rate of x^2 and y^2, respectively. Essentially at, say, $x = 10^3$, we need a time step less than $\delta t = 10^{-6}$, because the contribution of the kernel to this scale is 10^6. Thus, it is hard to perform a computation with the maximum mass size very large. For this reason, we have decided to limit the maximum mass to be $x = 10^3$ with $\gamma = 2$. Even for this case, after testing, we need to set time step as small as $\delta t = 10^{-7}$. Otherwise, the code produces a negative number density due to a huge conversion rate at large masses.

E2 Further Analyses

E2.1 The Case with $\gamma = 1$

In the case with $\gamma = 1$, it is shown in the main text that in additional to the similarity solution (22b), its "amplitude", ν, is predicted to follow an asymptotic tendency of Eq. (24). Thus, as $t \to \infty$, we expect that the distribution as a whole decreases with the rate $\sim t^{-1}$.

We examine whether the numerically–simulated rate of decrease of the distribution seen in Figs. 3 and 4 quantitatively agrees with this prediction. Here, it is not quite easy to measure the "whole" magnitude of the distribution that follows the similarity solution, because the similarity range increases with time, as seen in both figures. For the purpose here, we simply measure the whole magnitude of the distribution by its maximum value: this definition is expected to work well, because we see both in Figs. 3 and 4 that the the distribution maximum always marks the lower end of the similarity range. The result is plotted in Fig. E1 for the cases with $\lambda = 2$ and $\mu = 1$ (solid), $\lambda = 3$ and $\mu = 2$ (long dash), and $\lambda = 4$ and $\mu = 3$ (short dash) for the initial gamma distribution: the first and third curves correspond, respectively, to Figs. 3 and 4. All the three curves overlap very well, and we cannot see differences unless we zoom up the plot exten-

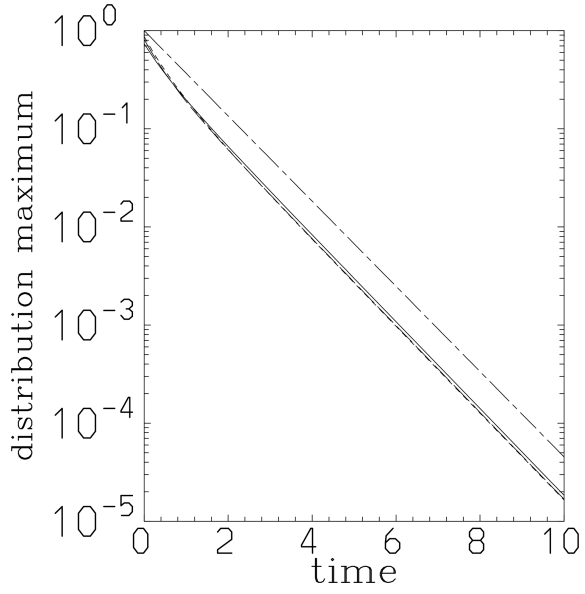

Figure E1. Plot of the maximum of the distribution, n, as a function of time for the case with $\gamma = 1$, $K = x + y$, and the parameter choices of the initial gamma distributions: $\lambda = 2$ and $\mu = 1$ (solid), $\lambda = 3$ and $\mu = 2$ (long dash), and $\lambda = 4$ and $\mu = 3$ (short dash). Also added is a curve of e^{-t} as chain dash.

sively: it suggests that regardless of the initial condition, the distribution evolve in a universal manner, and the decay of the distribution with time is clearly exponential, rather than algebraic as expected from Eq. (24). The time scale, τ, for the exponential is approximately, $\tau = 1$, as supported by a supplemental curve for $e^{-t/\tau}$ (chain dash).

Discrepancy with the simple simple similarity solution (22b) suggest that we need to invoke a full set of symmetry solutions considered in the Appendix D. Therein we show that Eq. (D25) is a possible alternative similarity solution with $\gamma = 1$, which explicitly suggests an exponential decay with time. Under this form, let's assume that its spatial dependence takes the form

$$n \sim x^{-\beta'}, \tag{E1}$$

where we expect a constant to be $\beta' \simeq 2$ based on the analysis of the main text. By consistency, $\nu(\xi)$ in Eq. (D25) must satisfy

$$\nu \sim \xi^{-\beta'}. \tag{E2}$$

Recalling that $\xi = xe^{-t/t_0}$, substituting Eq. (E2) into Eq. (D25), we obtain:

$$n = x^{-\beta'} e^{-t/\tau}, \tag{E3a}$$

where

$$\frac{1}{\tau} = \frac{2-\beta'}{t_0}. \tag{E3b}$$

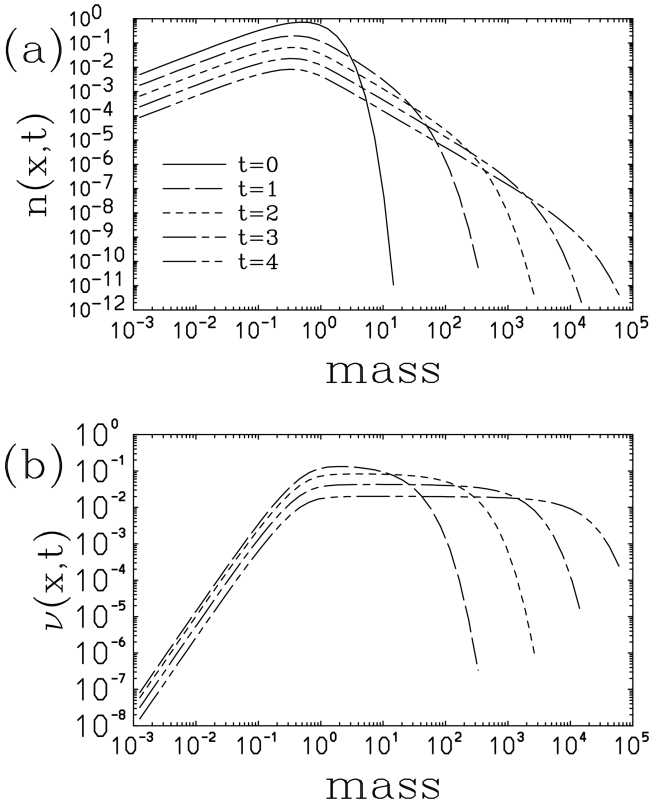

Figure E2. The case with $\gamma = 1$, $K = x + y$, initialized by the gamma distribution (Eqs. D26a, D26b) with $\lambda = 2$ and $\mu = 1$: the same as Fig. 3 but setting $\nu = nx^{\beta'}$ with $\beta' = 1.5$

Thus, to obtain an exponentially decaying solution, we need to assume, $\beta' < 2$, that is the case in the present simulations. From Fig. E1, we know $\tau \simeq 1$, thus we also conclude $t_0 \simeq 2 - \beta'$.

It transpires that a slight deviation of β' from the value 2 is crucial to ensure an exponentially decaying solution. Thus, we next estimate the value of β' by a revised versions of Figs. 3 and 4, in which the distributions are normalized by the factor $x^{-\beta'}$ instead with $\beta' \neq 2$. Figure E2 shows the same as Fig. 3, but re–setting to $\nu = nx^{\beta'}$ with $\beta' = 1.5$. The same analysis is also repeated with the other two cases with $\lambda = 3$ and $\mu = 2$, and $\lambda = 4$, $\mu = 3$. All those results confirm that the distributions asymptotically approach to the form with $\sim x^{-\beta'}$ with time with a value of $\beta' \simeq 1.5$ more precisely.

By combing this last result with the tendency of $n \sim e^{-t}$, we find that the numerical solution asymptotically approaches to the similarity solution given by Eq. (D50c). The last step is to more directly verify the validity of the full distribution solution (Eq. D47), setting $\beta = 1$ therein, so that it reads:

$$\nu = n(x,t)e^{4t}, \tag{E4a}$$

$$\xi = xe^{-2t}, \tag{E4b}$$

thus

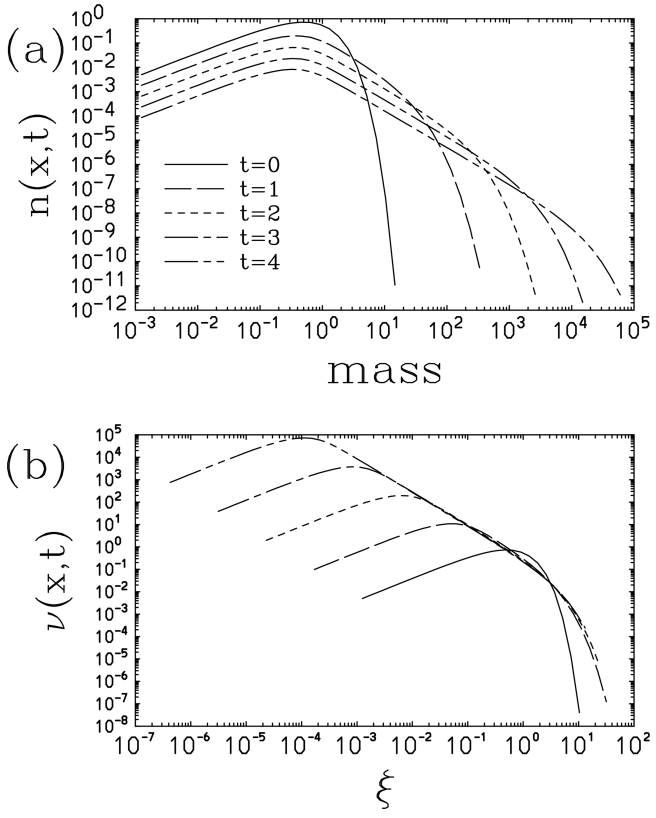

Figure E3. The case with $\gamma = 1$, $K = x + y$, initialized by the gamma distribution (Eqs. D26a, D26b) with $\lambda = 2$ and $\mu = 1$: the same as Fig. E2, but with the rescaling $v = ne^{4t}$ and $\xi = xe^{-2t}$.

$$v = \frac{\xi^{-3/2} e^{-\xi/4}}{2\sqrt{\pi}}, \tag{E4c}$$

if the solution (Eq. D47) is valid.

Figure E3b plots v defined by Eq. (E4a) against ξ defined by Eq. (E4b): we see that all the last four curves over $t =$ 1–4 overlap each other well. We also identify the algebraic regime with $\sim \xi^{-3/2}$ approximately over $x = 10^{-4}$–1, and the exponential regime with $\sim e^{-\xi/4}$ beyond $x = 1$.

E2.2 The Case with $\gamma = 2$

The case with $\gamma = 2$ is difficult to perform for the reason described in Sect. E1. For this reason, the upper end of the computation domain is limited to $x = 10^3$. This limitation also makes the obtained numerical results rather limited. The purpose of this subsection is to address those issues.

The most prominent feature expected for the case with $\gamma = 2$ is gelation or self–collapse of the distribution at a finite time, t_c, with a tendency of $(t_c - t)^2$. However, the obtained numerical results shown in Figs. 5 and 6 do not present such a finite time collapse, but it appears to continue to decay perpetually. To examine this tendency closely, we plot in Fig. E4

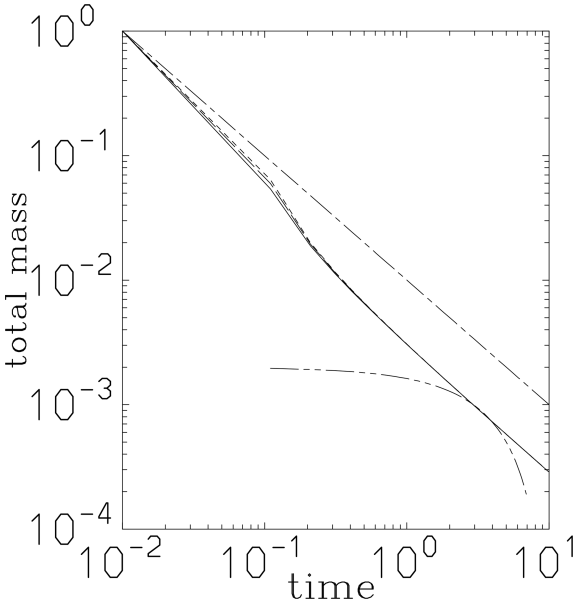

Figure E4. Time evolution of the total mass, m, for the case with $\gamma = 2$, $K = x^2 + y^2$, and the parameter choices of the initial gamma distributions: $\lambda = 2$ and $\mu = 1$ (solid), $\lambda = 3$ and $\mu = 2$ (long dash), and $\lambda = 4$ and $\mu = 3$ (short dash). Also added is a curve of τ/t with $\tau = 10^{-2}$ as chain dash, as well as a local fit of the curve of the form $\sim (t_c - t)^2$ around $t = 3$ with the double–chain dash curve with $t_c = 10$.

the time evolution of total mass, m, of the droplet distribution (Eq. 2) with three simulations with the kernel, $\gamma = 2$ and $K = x^2 + y^2$. More specifically, we consider the three initial conditions: $\lambda = 2$ and $\mu = 1$ (solid), $\lambda = 3$ and $\mu = 2$ (long dash), and $\lambda = 4$ and $\mu = 3$ (short dash) for gamma distributions: the first and third curves correspond, respectively, to Figs. 5 and 6. As in the case with Fig. E1, all those three curves match each other well, suggesting a universal evolution of the system: the total mass, m, decreases with time approximately following the tendency $\sim t^{-1}$, as suggested by a supplementary curve (chain dash).

An algebraic decay makes sense intuitively, considering a finite range of the droplet mass considered with the maximum, $x = 10^3$: due to a finite domain for the computation, the coalesce efficiency effectively remains constant with time, leading to such an algebraic decay. Here, since the total mass, m, is no longer conserved, it is possible to directly apply the solution with separation of variables derived in the Appendix C, where the time evolution is shown to follow Eq. (C4). The tendency of $\sim t^{-1}$ is recovered by taking the limit of $\chi t \gg 1$.

On the other hand, when an infinite domain is considered, the tail of distribution would continuously stretch upscales, and the coalescence efficiency increases with time due the fact that those very large droplets at the tail can more efficiently collect smaller droplets: it is intuitive to expect that

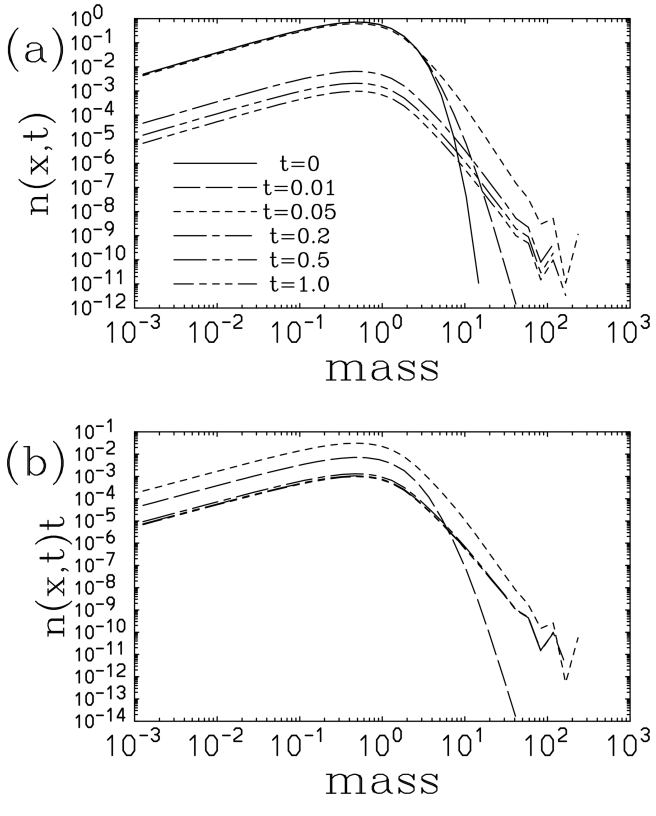

Figure E5. The case with $\gamma = 2$, $K = x^2 + y^2$, initialized by the gamma distribution (Eqs. D26a, D26b) with $\lambda = 2$ and $\mu = 1$: the same as Fig. 5, but in **(b)**, the number density multiplied by time, $n(x,t)t$; is plotted against x.

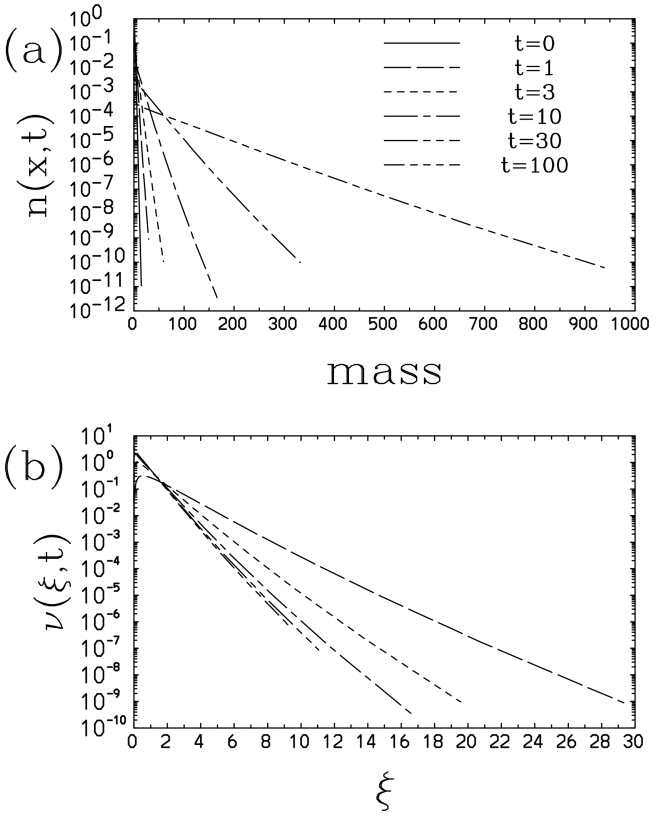

Figure E6. The same as Fig. 1, but with the linear scale for the horizontal axis.

such a chain process leads to a collapse of droplet distribution, as predicted mathematically.

Finally, although the actual decay of the total mass hardly follow the curve, $(t_c - t)^2$, it is still possible to locally fit the time series of m to the form $(t_c - t)^2$. An example of such a local fit is shown by a double–chain dash curve in Fig. E4: although the range of fit is not very extensive, say only over $t = 2$–5, that explains a reasonable collapse of curves by this method in Figs. 5 and 6.

The curves in Fig. E4 are not totally algebraic, but present a well–marked kink with a sudden drop around $t = 10^{-1}$: this roughly corresponds to the time that the distribution tail reaches the maximum, $x = 10^3$, of the computational, as seen in Figs. 5 and 6. Arguably, beyond this point, a real algebraic decay sets on. Onset of such an algebraic decay would be continuously delayed, when a larger computational domain is considered. Finally, the same as Fig. 5, but showing the curve with renormalization by $\nu = n(x,t)t$ in the second frame (b), is shown in Fig. E5: the curves collapse well above $t = 0.2$.

E2.3 The Case with $\gamma = 0$

In the case with $\gamma = 0$ and $K = 1$, the general similarity solution is given by Eq. (21a), and the analysis of Appendix D4.3 further shows that the formal solution (D42) presents the asymptotic tendency,

$$n(x,t) \to \frac{4}{t^2} e^{-2x/t}, \tag{E5}$$

thus $\nu(\xi) \sim e^{-2\xi}$, where $\xi = x/t$. This solution can easily be verified visually by re–plotting Figs. 1 and 2 in the linear scale for the horizontal axis, as shown in Fig. E6 for the former: above $t = 10$, the distribution of ν is well collapsed into a single straight line with this linear–log plot.

E3 Asymptotic Convergence of Numerical Solutions

Over the last section, we have examined the asymptotic tendencies of the obtained numerical results in comparisons with more exact similarity solution identified in the Appendix D. The purpose of this section is to quantify the tendency that the numerical solutions converge into those asymptotic solutions. For this purpose, we re–write the

numerically–simulated solutions as

$$n(x,t) = \frac{\nu(\xi,t)}{t^2}, \tag{E6a}$$

$$n(x,t) = \xi^{-3/2} e^{-4t} \nu(\xi,t) \tag{E6b}$$

for $\gamma = 0$ and $\gamma = 1$, respectively, where the transformed "mass" is defined by

$$\xi = x/t, \tag{E7a}$$

$$\xi = x e^{-2t}, \tag{E7b}$$

respectively. Here, an extra factor, $\xi^{-3/2}$ is multiplied on $\nu(\xi,t)$ in Eq. (E6b), compared to the previous definition (E4a), so that the singularity of $\nu(\xi,t)$ as $\xi \to 0$ can be avoided.

In both cases, we expect the numerical solutions asymptotically approach to the similarity solution, $\nu_\infty(\xi)$, i.e. $\nu(\xi) \to \nu_\infty(\xi)$ as $t \to +\infty$. Recall that the asymptotic solutions are given by

$$\nu_\infty(\xi) = 4e^{-2\xi} \tag{E8a}$$

$$\nu_\infty(\xi) = \frac{e^{-\xi/4}}{2\sqrt{\pi}}, \tag{E8b}$$

respectively, for $\gamma = 0$ and $\gamma = 1$.

We measure the error, ε, by the root–square measure defined by

$$\varepsilon = \| \nu(\xi,t) - \nu_\infty(\xi) \|^{1/2}, \tag{E9}$$

where the integral for the norm is performed in respect to ξ. The results are shown in Fig. E7 for the cases with (a) $\gamma = 0$ and (b) $\gamma = 1$, and three initialization with the gamma distributions: $\lambda = 2$ and $\mu = 1$ (solid), $\lambda = 3$ and $\mu = 2$ (long dash), and $\lambda = 4$ and $\mu = 3$ (short dash). In the case with $\gamma = 0$, the asymptotic error, ε, defined by Eq. (E9) decreases with time. However, this tendency towards the converged solution is rather slow, approximately following an algebraic curve with $\sim t^{-1/2}$. Also the convergence rate becomes slightly slower with the increasing λ and μ.

In the case with $\gamma = 1$, on the other hand, the asymptotic error (Eq. E9) decreases initially, up to the time, $t \sim 4$, then it turns to increase with time, but with an indication of asymptotically approaches to the value around 0.1. Causes for such a divergent tendency can be traced in the following manner: initially, the error decreases as the algebraic range with $\sim \xi^{-3/2}$ stretches to downscales with time, as seen in Fig. E3b. However, the rate of this downscale stretch decreases with time, thus the rate of decrease of error also decreases. As a whole, in this manner, the average of ν increases over time, and as a result, the same degree of error relative to ν is increasingly amplified with the increasing ν. As $t \to +\infty$, $\xi \to 0$, and $\nu \to 1/2\sqrt{\pi}$, thus leading to a comparison between a constant and a constant. Here, a closer examination of Fig. E3b reveals that the algebraic

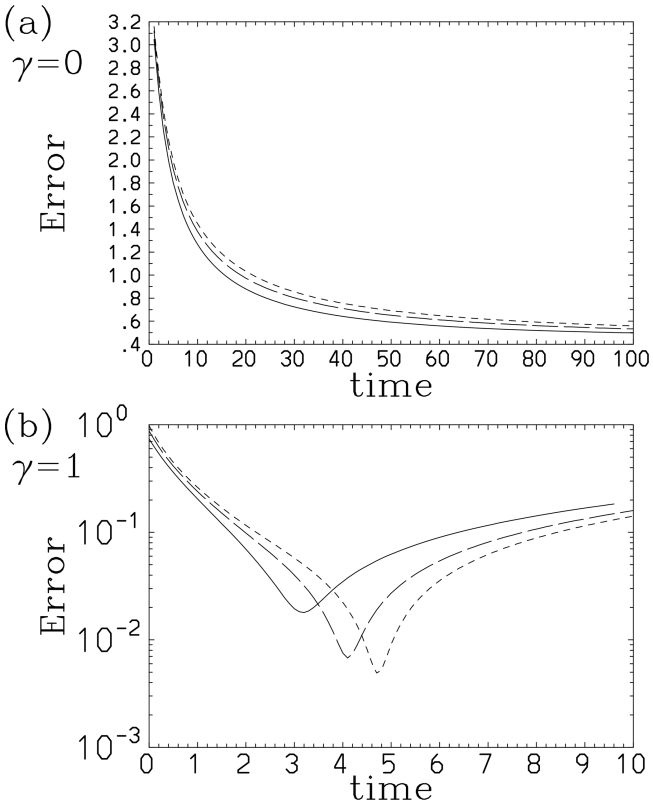

Figure E7. Time evolution of the asymptotic error, ε, defined by Eq. (E9) for the cases with **(a)** $\gamma = 0$, $K = 1$ and **(b)** $\gamma = 1$, $K = x + y$, and with the three initializations with the gamma distributions: $\lambda = 2$ and $\mu = 1$ (solid), $\lambda = 3$ and $\mu = 2$ (long dash), and $\lambda = 4$ and $\mu = 3$ (short dash).

slope presents a slight tendency of increasing with time, thus leading to an increase of error beyond $t \sim 4$. We interpret that this tendency is due to a finite spectrum range in computations: as the algebraic tail stretches upscale, the distribution begins to feel the upper end of spectrum considered, and the transfer of mass upscales by coalescence gradually becomes "blocked" at the upper end. This interpretation is consistent with the fact that the point of minimum error delays with the increasing λ and μ, because those parameters make the initial peak steeper, delaying the timing beginning to feel the upper bound.

Code and data availability. All the Fortran codes and data used for the present study is available from Yano (2026).

Author contributions. The present study has been envisioned by MPHA, and principally performed by JIY with extensive inputs by MW.

Competing interests. The contact author has declared that none of the authors has any competing interests.

Disclaimer. Publisher's note: Copernicus Publications remains neutral with regard to jurisdictional claims made in the text, published maps, institutional affiliations, or any other geographical representation in this paper. The authors bear the ultimate responsibility for providing appropriate place names. Views expressed in the text are those of the authors and do not necessarily reflect the views of the publisher.

Acknowledgements. The numerical code for SCE has been kindly provided by Andreas Bott. We much appreciate the critical, constructive comments by the anonymous Referee #1.

Review statement. This paper was edited by Jinqiao Duan and reviewed by two anonymous referees.

References

Barenblatt, G. I.: Scaling, Self-Similarity, and Intermediate Asymptotics, Cambridge University Press, Cambridge, UK, 386 pp., ISBN-13 978-1316980279, 1996.

Bender, C. M., and Orszag, S. A.: Advanced Mathematical Methods for Scientists and Engineers, McGraw-Hill, New York, 593 pp., ISBN-10 007004452X, 1978.

Berry, E. X.: Cloud droplet growth by collection, J. Atmos. Sci., 24, 688–701, https://doi.org/10.1175/1520-0469(1967)024<0688:CDGBC>2.0.CO;2, 1967.

Berry, E. X. and Reinhardt, R. L.: An analysis of cloud drop growth by collection: Part I. Double distribution, J. Atmos. Sci., 31, 1814–1824, https://doi.org/10.1175/1520-0469(1974)031<1814:AAOCDG>2.0.CO;2, 1974a.

Berry, E. X. and Reinhardt, R. L.: An analysis of cloud drop growth by collection: Part II. Single initial distribution, J. Atmos. Sci., 31, 1825–1831, https://doi.org/10.1175/1520-0469(1974)031<1825:AAOCDG>2.0.CO;2, 1974b.

Berry, E. X. and Reinhardt, R. L.: An analysis of cloud drop growth by collection: Part III. Accretion and self–collection, J. Atmos. Sci., 31, 2118–2126, https://doi.org/10.1175/1520-0469(1974)031<2118:AAOCDG>2.0.CO;2, 1974c.

Berry, E. X. and Reinhardt, R. L.: An analysis of cloud drop growth by collection: Part IV. A new parameterization, J. Atmos. Sci., 31, 2127–2135, https://doi.org/10.1175/1520-0469(1974)031<2127:AAOCDG>2.0.CO;2, 1974d.

Bluman, G. W. and Kumei, S.: Symmetries and Differential Equations, Springer, New York, 412 pp., ISBN-10 3540969969, 1989.

Bott, A.: A flux method for the numerical solution of the stochastic collection equation, J. Atmos. Sci., 55, 2284–2293, https://doi.org/10.1175/1520-0469(1998)055<2284:AFMFTN>2.0.CO;2, 1998.

Drake, R. L.: The scalar transport equation of coalescence theory: Moments and kernels. J. Atmos. Sci., 29, 537–547, https://doi.org/10.1175/1520-0469(1972)029<0537:TSTEOC>2.0.CO;2, 1972.

Escobedo, M., Mischler, S., and Perthame, B.: Gelation in coagulation and fragmentation models, Comm. Math. Phys., 231, 157–188, https://doi.org/10.1007/s00220-002-0680-9, 2002.

Friedlander, S. K.: Theoretical considerations for the particle size spectrum of stratospheric aerosol, J. Meteor., 18, 753–759, https://doi.org/10.1175/1520-0469(1961)018<0753:TCFTPS>2.0.CO;2, 1961.

Fournier, N. and Laurençot, P.: Existence of self–similar solutions to Smoluchowski's coagulation equation, Comm. Math. Phys., 256, 589–609, https://doi.org/10.1007/s00220-004-1258-5, 2005.

Fournier, N. and Laurençot, P.: Well-posedness of Smoluchowski's coagulation equation for a class of homogeneous kernels, J. Funct. Anal., 233, 351–379, https://doi.org/10.1016/j.jfa.2005.07.013, 2006a.

Fournier, N. and Laurençot, P.: Local properties of self-similar solutions to Smoluchowski's coagulation equation with sum kernels, Proc. Roy. Soc. Edinburgh A, 136, 485–508, https://doi.org/10.1017/S0308210500005035, 2006b.

Golovin, A. M.: The solution of the coagulation equation for cloud droplets in a rising air current, Izv. Akad. Nk. SSSR (Geophys. Ser.) (English translation), 5, 482–487, 1963.

Grigoriev, Y. N. and Meleshko, S. V.: Group analysis of kinetic equations, Russ. J. Numer. Anal. Math. Modeling, 10, 425–447, https://doi.org/10.1515/rnam.1995.10.5.425, 1995.

Grigoriev, Y. N., Ibragimov, N. H., Kovalev, V. F., and Meleshko, S. V.: Symmetries of Integro–Differential Equations: With Application in Mechanics and Plasma Physics, Springer, Heidelberg, 305 pp., ISBN-13 978-90-481-3796-1, https://doi.org/10.1007/978-90-481-3797-8, 2010.

Grabowski, W. W., Morrison, H., Shima, S., Abade, G. C., Dziekan, P., and Pawlowska, H.: Modeling of cloud microphysics: Can we do better?, B. Am. Meteorol. Soc., 100, 655–672, https://doi.org/10.1175/BAMS-D-18-0005.1, 2019.

Kingston, J. G. and Sophocleous, C.: On form–preserving point transformation of partial differential equations, J. Phys. A Math. Gen, 31, 1597–1619, https://doi.org/10.1088/0305-4470/31/6/010, 1998.

Leyvraz, F.: Scaling theory and exactly solved models in the kinetics of irreversible aggregation, Phys. Rep., 383, 95–212, https://doi.org/10.1016/S0370-1573(03)00241-2, 2003.

Lin, F., Yang, Y., Yang, X., and Zhang, Q.: Preliminary group classification and exact solutions of Smoluchowski equation with a source, J. Comput. App. Math., 444, 115770, https://doi.org/10.1016/j.cam.2024.115770, 2024.

Long, A. B.: Solutions to the droplet collection equation for polynomial kernels, J. Atmos. Sci., 31, 1040–1052, https://doi.org/10.1175/1520-0469(1974)031<1040:STTDCE>2.0.CO;2, 1974.

Menon, G. and Pego, R. L.: Approach to self–similarity in Smoluchowski's coagulation equations, Comm. Pure Appl. Math., LVII, 1197–1232, https://doi.org/10.1002/cpa.3048, 2004.

Pruppacher, H. R. and Klett, J. D.: Microphysics of Clouds and Precipitation, Second Revised and Enlarged Edition with an Introduction to Cloud Chemistry and Cloud Electricity, Kluwer Academic Publishers, Dordrecht, 954 pp., ISBN-10 0792342119, 1997.

Schumann, T. E.: Theoretical aspects of the size distribution of fog particles, Q. J. Roy. Meteor. Soc., 66, 195–207, https://doi.org/10.1002/qj.49706628508, 1940.

Scott, W. T.: Analytic studies of cloud droplet coalescence I, J. Atmos. Sci., 25, 54–65, https://doi.org/10.1175/1520-0469(1968)025<0054:ASOCDC>2.0.CO;2, 1968.

Smoluchowski, M.: Versuch einer mathematischen Theorie der Koagulationskinetik kolloider Lösungen, Z. Phys. Chem., 92, 129–168, https://doi.org/10.1515/zpch-1918-9209, 1917.

Sorbjan, Z.: Structure of the Atmospheric Boundary Layer, Prentice Hall, Englewood Cliffs, USA, 317 pp., ISBN 0138535574, 9780138535575, 1989.

Srivastava, R. C.: On the scaling of equations governing the evolution of droplet size distribution, J. Atmos. Sci., 45, 1091–1092, https://doi.org/10.1175/1520-0469(1988)045<1091:OTSOEG>2.0.CO;2, 1988.

Twomey, S.: Statistical effects in the evolution of a distribution of cloud droplets by coalescence, J. Atmos. Sci., 21, 553–557, https://doi.org/10.1175/1520-0469(1964)021<0553:SEITEO>2.0.CO;2, 1964.

Twomey, S.: Computations of rain formation by coalescence, J. Atmos. Sci., 23, 405–411, https://doi.org/10.1175/1520-0469(1966)023<0405:CORFBC>2.0.CO;2 , 1966.

van Dongen, P. G. J. and Ernst, M. H.: Scaling solutions of Smoluchowski's coagulation equation, J. Stat. Phys., 50, 295–329, 1988.

Wacławczyk, M., Grebenev, V. N. and Oberlack, M.: Lie symmetry analysis of the Lundgren–Monin–Novikov equations for multipoint probability density functions of turbulent flow, J. Phys. A Math. Theor., 50, 175501, https://doi.org/10.1088/1751-8121/aa62f4, 2017.

Xie, M.: Comment on "Theoretical aspects of the size distribution of fog particles", Q. J. Roy. Meteor. Soc., 150, 3196–3200, https://doi.org/10.1002/qj.4730, 2024.

Yano, J.-I.: Instruction for Downloading the Codes and Data used in "Stochastic Collection Equation: Invariant Evolution of the Cloud Droplet–Size Distribution", hal-05830449, https://hal.science/hal-05830449 (last access: 23 November 2026), 2026.